Genetic dissection of the different roles of hypothalamic kisspeptin neurons in regulating female reproduction

Luhong Wang[1], Charlotte Vanacker[1], Laura L. Burger[1], Tammy Barnes[2], Yatrik M. Shah[1], Martin G. Myers[1,2], Suzanne M. Moenter[1,2,3*]

Departments of Molecular and Integrative Physiology[1], Internal Medicine[1] and Obstetrics & Gynecology[3], University of Michigan, Ann Arbor, MI 48109

*Requests for materials and correspondence, Suzanne M. Moenter, smoenter@umich.edu

The authors have nothing to disclose

Abstract

The brain regulates fertility through gonadotropin-releasing hormone (GnRH) neurons. Estradiol induces negative feedback on pulsatile GnRH/luteinizing hormone (LH) release and positive feedback generating preovulatory GnRH/LH surges. Negative and positive feedback are postulated to be mediated by kisspeptin neurons in arcuate and anteroventral periventricular (AVPV) nuclei, respectively. Kisspeptin-specific ERα knockout mice exhibit disrupted LH pulses and surges. This knockout approach is neither location-specific nor temporally-controlled. We utilized CRISPR-Cas9 to disrupt ERα in adulthood. Mice with ERα disruption in AVPV kisspeptin neurons have typical reproductive cycles but blunted LH surges, associated with decreased excitability of these neurons. Mice with ERα knocked down in arcuate kisspeptin neurons showed disrupted cyclicity, associated with increased glutamatergic transmission to these neurons. These observations suggest activational effects of estradiol regulate surge generation and maintain cyclicity through AVPV and arcuate kisspeptin neurons, respectively, independent from its role in the development of hypothalamic kisspeptin neurons or puberty onset.

Introduction

Infertility is a common clinical problem affecting 15% of couples; ovulatory disorders account for 25% of this total(Macaluso et al., 2010). The hypothalamic-pituitary-gonadal axis controls reproduction and malfunction of this axis can cause ovulatory dysfunction and/or other disturbances of the reproductive cycle (Helm et al., 2009; Plant and Zeleznik, 2015). Gonadotropin-releasing hormone (GnRH) neurons form the final common pathway for central neural regulation of reproduction. GnRH stimulates the pituitary to secrete follicle-stimulating hormone and luteinizing hormone (LH), which regulate gonadal steroid and gamete production. Estradiol, via estrogen receptor alpha (ERα), plays crucial roles in both homeostatic negative feedback and positive feedback action on GnRH/LH release in females (Docke and Dörner, 1965; Moenter et al., 1990; Lubahn et al., 1993; Krege et al., 1998; Wintermantel et al., 2006; Christian et al., 2008; Glanowska et al., 2012; Cheong et al., 2015). Low estradiol levels suppress pulsatile GnRH/LH release, whereas sustained elevations in estradiol during the late follicular phase of the cycle cause a switch of estradiol feedback action from negative to positive, inducing prolonged GnRH/LH surges, which ultimately triggers ovulation (Christian and Moenter, 2010). As GnRH neurons typically do not express detectable ERα (Hrabovszky et al., 2001), estradiol feedback is likely transmitted to GnRH neurons by ERα-expressing afferents.

Kisspeptin neurons in the arcuate and anteroventral periventricular (AVPV) regions are estradiol-sensitive GnRH afferents that are postulated to mediate estradiol negative and positive feedback, respectively (Oakley et al., 2009; Lehman et al., 2010). Kisspeptin potently stimulates GnRH neurons and *Kiss1* mRNA is differentially regulated in these nuclei by estradiol (Han et al., 2005; Messager et al., 2005; Smith et al., 2005; Pielecka-Fortuna et al., 2008; Lehman et al., 2010; Kumar et al., 2015; Yip et al., 2015). ERα in kisspeptin cells is critical for estradiol negative and positive feedback, as kisspeptin-specific ERα knockout (KERKO) mice exhibit higher frequency LH pulses and fail to exhibit estradiol-induced LH surges (Mayer et al., 2010; Dubois et al., 2015; Greenwald-Yarnell et al., 2016; Wang et al., 2018). Although informative, the KERKO model has several caveats that limit interpretation. First, ERα is deleted as soon as *Kiss1* is expressed, before birth in arcuate kisspeptin neurons (also called KNDy neurons for coexpression of kisspeptin, neurokinin B and dynorphin) and before puberty in AVPV kisspeptin neurons (Semaan et al., 2010; Kumar et al., 2014). This may cause developmental changes in these cells and/or their networks. Second, ERα is deleted from all kisspeptin cells, thus making it impossible to assess independently the role of AVPV and arcuate kisspeptin neurons.

Combining CRISPR-Cas9 with targeted viral vector injection allows deletion of ERα in a nucleus-specific and temporally-controlled manner to address the above caveats (Swiech et al., 2014). We designed cre-dependent AAV vectors that carry single guide RNAs (sgRNAs) that target *Esr1* (encoding ERα) or *lacZ* and delivered these vectors to the AVPV or arcuate of adult female mice that express Cas9 in kisspeptin cells. We then compared the reproductive phenotypes as well as kisspeptin neuronal physiology in AAV-*Esr1* vs AAV-*lacZ* targeted mice and KERKO mice.

Results

AVPV kisspeptin neurons from KERKO mice exhibit decreased firing rate and excitability.

We first used extracellular recordings to monitor the spontaneous firing rate of YFP-identified AVPV kisspeptin neurons in coronal brain slices from ovary-intact control and KERKO mice. As the persistent cornified vaginal cytology of KERKO mice is similar to that observed during estrus (Greenwald-Yarnell et al., 2016), we used mice in the estrous stage of the reproductive cycle as controls. The firing frequency of AVPV kisspeptin neurons was lower in ovary-intact KERKO mice compared to controls (Figure 1a, b, two-way ANOVA/Holm-Sidak, p=0.0001). To test if the firing rate of AVPV kisspeptin neurons in KERKO mice responds to circulating estradiol, we repeated this study in ovariectomized (OVX) mice and OVX mice with an estradiol implant producing constant physiologic levels (OVX+E)(Christian et al., 2005). OVX reduced and

estradiol treatment increased firing rate in cells from control, but not KERKO, mice (Figure 1a, b two-way ANOVA/Holm-Sidak, control intact vs OVX p=0.009, intact vs OVX+E, p=0.02, OVX vs OVX+E, p<0.0001). As a result of this difference, the firing frequency is higher in cells from OVX+E control than OVX+E KERKO mice (p<0.0001). Statistical test parameters for all figures are in Tables 1 and 2.

We next recorded the whole-cell firing signatures of neurons in these six groups in response to current injection. AVPV kisspeptin neurons in control mice mice exhibit a greater number of depolarization-induced bursts (DIB) and rebound bursts when estradiol is elevated, confirming previous observations(Wang et al., 2016) (Figure 1c, d, e, Chi-square, DIB, p=0.02; rebound, p=0.02; Fisher's exact *post hoc* test, DIB, OVX vs OVX+E, p=0.008, rebound OVX vs OVX+E p=0.03, for other paired comparisons, p>0.2)). In KERKO mice, these two types of bursts were rare (<25% of cells) in all steroid conditions tested and were not regulated by estradiol (Figure 1c, d, e, Chi-square, DIB, p=0.4, rebound, p=0.3). We also compared the action potential output of these cells in response to current injection (0-50 pA, 10 pA increments, 500 ms). Cells from ovary-intact KERKO mice generated fewer action potentials compared to controls. Action potential generation as a function of current injection was similar in cells from OVX control and OVX KERKO mice but was increased by estradiol only in control mice (Figure 1f, two-way repeated-measures ANOVA/Holm-Sidak, intact, 20 pA, p=0.03, 30 pA, p=0.06; OVX+E, 20 pA to 50 pA, p≤0.04). Reduced action potential firing of AVPV kisspeptin neurons from KERKO mice may be attributable at least in part to decreased input resistance compared to controls (Figure1-figure supplement 1, two-way ANOVA/Holm-Sidak control vs KERKO, intact, p=0.006, OVX, p=0.7, OVX+E p=0.02).

As both depolarization-induced bursts and rebound bursts are sensitive to NiCl (100 µM)(Lee et al., 1999) at levels that fairly specifically block T-type calcium channels, we measured T-type (I_T) current density and voltage dependence. I_T current density was decreased in AVPV kisspeptin cells from gonad-intact KERKO mice compared to controls (Figure 2a, b, two-way repeated-measures ANOVA/Holm-Sidak, -50 mV, p=0.003; -40 mV, p=0.002; -30 mV, p=0.003). The voltage dependence of activation was not different between groups, but the voltage dependence of inactivation was depolarized in cells from KERKO mice (Figure 2c, control vs KERKO, two-tailed unpaired Student's *t*-test, $V_{1/2}$ activation -52.2±1.6 vs -48.6±1.4 mV, p>0.1; slope 5.5±0.6 vs 5.5±0.7, p>0.1; $V_{1/2}$ inactivation -74.8±4.1 vs -61.9±3.1 mV, p=0.03; slope -3.1±0.5 vs -4.2±0.3, p=0.1).

Design and validation of sgRNAs that target *Esr1*.

A caveat of studying the role of ERα in AVPV kisspeptin neurons using KERKO mice is that the deletion of ERα (encoded by *Esr1*) using cre recombinase under the control of the kisspeptin promoter is neither time- nor location-specific. We utilized the CRIPSR-Cas9 approach to achieve temporal and spatial control of *Esr1* gene knockdown. Two sgRNAs were designed that target exon1 of *Esr1* based on software prediction (Ran et al., 2013); sites predicted by FengZhang's guide design software (http://crispr.mit.edu) as possible off-target regions for binding of these guides are listed in Table 3. The efficiency of each guide tested *in vitro* in C2C12 mouse myoblast cells (Milanesi et al., 2008). The sgRNAs that target *Esr1* and a sgRNA that targets *lacZ* as a control were subcloned into the lentiCRISPRv2 plasmid(Sanjana et al., 2014), from which Cas9 and the sgRNA are expressed after transfection of C2C12 cells. Puromycin was used to select construct-expressing cells. After a ~4-week selection period, DNA was harvested and the *Esr1* region sequenced. Cells expressing either of the sgRNAs targeting *Esr1,* but not *lacZ*, exhibited a peak-on-peak sequencing pattern, indicating disruption of the gene (Figure 3a). As these *in vitro* experiments suggested these sgRNAs were able to mutate *Esr1*, we designed Cre-dependent AAV vectors to express each sgRNA and mCherry (to indicate infected cells) under control of the U6 promoter (Figure 3b). The AAV vector was bilaterally stereotaxically injected into the AVPV region of adult female mice that express Cas9 and GFP under control of the kisspeptin promoter (*Kiss1*-Cre; *Cas9 loxp*-stop-*Gfp*, Figure3-figure supplement 1); these groups are referred to as AVPV-AAV-*Esr1* or AVPV-AAV-*lacZ*. Only one guide was injected per animal to allow comparison of phenotypes when different areas of *Esr1* were targeted. The ERα knockdown efficiency of the two sgRNAs target *Esr1* was comparable. The infection rate for AVPV-AAV-*Esr1* was 81±4% (Figure 3d, *Esr1*-guide 1 [g1] 82±2%, n=3; *Esr1*-guide 2 [g2] 81±8%, n=3,) and only 28±1% of AVPV kisspeptin cells expressed ERα post infection (Figure 3d, n=3, *Esr1*-guide1 27±0.4%, n=3 *Esr1*-guide2 28±2%). In mice that received AVPV-AAV-*lacZ* (n=3), the infection rate was comparable at 82±2%, but there was no disruption of ERα; 72±2% of AVPV kisspeptin neurons expressed ERα, which is similar to control mice (Kumar et al., 2015). Of note, the ERα antibody used recognizes the C-terminus, suggesting a lack of rare splice variants that were generated at low levels in initial ERKO mice (Couse et al., 1995).

Deletion of ERα in AVPV kisspeptin neurons in adulthood does not affect estrous cycles but disrupts preovulatory and estradiol-induced LH surges.

We monitored the reproductive cycles of the mice injected with AAV-sgRNAs in the AVPV 12 days before and for up to eight weeks following surgery. Neither AVPV-AAV-*Esr1* guide (tested independently) nor the AVPV-AAV-*lacZ* disrupted reproductive cyclicity (Figure 3e), even in mice with a high rate of bilateral infection (~80%). These mice entered proestrus at the same frequency in the last 4 weeks compared to the first 4 weeks (2 weeks pre-surgery + first 2 weeks post-surgery, two-way repeated-measures ANOVA/Holm-Sidak, before vs after, g1, n=3, 1.3±0.1 vs 1.6±0.1; g2, n=4, 1.2±0.1 1.4±0.1, *lacZ* n=4, 1.3±0.2 vs1.3±0.1, p>0.1 for each paired comparison). To test for the occurrence of estradiol positive feedback, we monitored both proestrous (preovulatory) and estradiol-induced LH surges in these mice. Surge data were similar for guide 1 and guide 2 and data from both guides were combined for group comparisons. Both proestrous and estradiol-induced LH surges were blunted after ERα knockdown (Figure 3f, g, two-way repeated-measures ANOVA/Holm-Sidak; g, *lacZ*, 3pm vs 5pm, p=0.04; *lacZ* vs *Esr1*, 4pm, p=0.006, 5 pm, p<0.0001, h, *lacZ* AM vs PM, p<0.0001). There were fewer corpra lutea (CL) in mice with *Esr1* guides targeted to the AVPV (p<0.05, guide 1 and 2 combined n=6, 5.2±2.1 CL/mouse, vs *lacZ* guide n=5, 10.8±0.4 CL/mouse, two-tailed paired Student's t test with Welch's correction, t=2.598, df=5.305). Of note, variation was high in the *Esr1* mice, with two looking similar to controls, two having fewer CL and two not having any CL. This suggests ovulation is disrupted in a substantial subpopulation of these mice but can proceed with the blunted LH surge in some animals.

Decreased excitability of AVPV kisspeptin neurons in AAV-*Esr1* knockdown mice.

To test if knockdown of ERα in adult AVPV kisspeptin neurons alters their intrinsic excitability, we recorded firing signatures of infected and uninfected cells in brain slices from AAV injected OVX+E mice. We again observed no difference between AVPV-AAV-*Esr1* g1 vs g2 and combined these data. Some cells were loaded with neurobiotin during recording for identification and ERα protein detected *post hoc* with immunofluorescence (Figure 4a, c, and IF *post hoc* portions of 4e-j). Cells not infected with AVPV-AAV-*Esr1* and cells infected with either AVPV-AAV-*Esr1* guide but in which ERα protein was detected exhibited similar firing signatures in terms of DIB and rebound bursts (Figure 4b, e, f). In contrast, cells infected by AVPV-AAV-*Esr1* that had undetectable ERα protein had reduced burst firing compared to AVPV-AAV-*lacZ* or uninfected groups (Figure 4e, f, Chi-square, DIB, p=0.008, rebound bursts, p=0.0008; Fisher's

exact *post hoc* test, DIB, *Esr1* vs *lacZ*, or vs uninfected, p≤0.03 ;rebound, *Esr1* vs *lacZ*, or vs uninfected p≤0.04; for other paired comparisons, p>0.5). The firing signature of AAV-*Esr1* infected cells with successful deletion of ERα was comparable to cells from KERKO mice (Chi-square, p>0.9 for both DIB and rebound bursts). Cells that lost detectable ERα after AVPV-AAV-*Esr1* infection also produced fewer action potentials with current injection than cells infected with AAV-*lacZ* (Figure 4d left and center, two-way repeated-measures ANOVA/Holm-Sidak, *Esr1* vs *lacZ,* 20 pA, p=0.08; 30 to 50pA p≤0.02). This difference is not attributable to passive properties (Figure 1- figure supplement 1a,b). The relationship between current injection and number of action potentials fired (input-output curve) in cells from KERKO and in AVPV-AAV-*Esr1* knockdown mice was only different at the highest level of current injected, with AVPV-AAV-*Esr1* infected cells being less excitable (Figure 4d, right, two-way repeated-measures ANOVA/Holm-Sidak, 50pA, p=0.01), despite no change in input resistance (Figure 1-figure supplement 1a,b KERKO vs AAV, p=0.08). Action potential properties from AVPV-AAV-*Esr1* knockdown cells with AVPV-AAV-*lacZ* control also differed. Specifically, loss of ERα led to decreased action potential rate of rise, a trend towards prolonged full-width half-maximum (FWHM), and hyperpolarized afterhyperpolarization potential (AHP) (Figure 4g, h, j, two-tailed unpaired Student's *t*-test, h, p=0.02, j, p=0.0002; i, Mann-Whitney U-test, p=0.06).

In parallel, we performed whole-cell patch-clamp recording with single-cell PCR *post hoc* identification of *Esr1* mRNA on a separate set of cells (AVPV-AAV-*Esr1* 10 cells from 4 mice, AVPV-AAV-*lacZ*, 9 cells from 3 mice; primers are in Table 4). A similar decrease in burst firing and action potential input-output curve was observed in *Esr1* mRNA negative cells as was observed in cells verified to have undetectable ERα protein by immunofluorescence (Figure 4e, f, Chi-square, DIB, p=0.04, rebound p=0.03; Fisher's exact *post hoc* test, DIB, *Esr1* vs *lacZ* p=0.03. *Esr1* vs uninfected, p=0.07; rebound, *Esr1* vs *lacZ* p=0.02; for other paired comparisons, p>0.2). Absence of *Esr1* mRNA expression was again associated with decreased number of action potentials in response to current injection (Figure 4e middle, *Esr1* vs *lacZ,* p<0.002 for 20 to 50pA steps*)*. Absence of *Esr1* mRNA, similar to loss of ERα protein, led to decreased action potential rate of rise, prolonged FWHM, and AHP (Figure 4g-j right, two-tailed unpaired Student's *t*-test, h, p=0.02; i, p=0.006, j, p=0.02). Single-cell PCR analysis also indicates that a lower percent of AVPV-AAV-*Esr1* knockdown cells express *Kiss1* and a trend to increase in *Esr2* mRNA (AVPV-AAV-*Esr1* 23 cells from 4 mice, AVPV-AAV-*lacZ*, 16 cells from 3 mice, Figure 4- figure supplement 1). Interestingly, expression of the mRNA for progesterone receptor (*Pgr)* did not differ between groups (Figure 4- figure supplement 1), suggesting the

estradiol-dependence of this gene may be paracrine regulated in the brain as in other tissues(Hilton et al., 2015). We also examined gene expression for several ion channels, but none showed any changes or patterns of expression among groups (Figure 4- figure supplement 1).

Deletion of ERα in arcuate kisspeptin neurons in adulthood disrupted estrous cycles.

To examine the role of estradiol feedback on arcuate kisspeptin neurons, we delivered the AAV-sgRNAs bilaterally to the arcuate region to knockdown ERα in these cells (Figure 5-figure supplement 1); these groups are referred to as Arc-AAV-*Esr1* or Arc-AAV-*lacZ*. The infection rate for Arc-AAV-*Esr1* was 92±3% (Figure 5-figure supplement 1, n=3, *Esr1*-guide1 96±2%, n=3 *Esr1*-guide2 86±2%) and only 34±3% of KNDy neurons expressed ERα post infection (Figure 5a n=3, *Esr1*-g1 38±0.3%, n=3 *Esr1*-g2 30±5%). In mice that received Arc-AAV-*lacZ*, the infection rate was comparable (Figure 5a n=3 94±3%), and 92±1% of KNDy neurons expressed ERα, similar to control mice (Kumar et al., 2015). Reproductive cycles were monitored for 12 days before and for up to eight weeks following surgery. In contrast to mice with Arc-AAV-*Esr1* targeted to the AVPV region, mice with the same virus targeted to the arcuate began exhibiting disrupted cyclicity three to four weeks post surgery (Figure 5b). These mice entered proestrus less frequently after surgery than before (two weeks pre-surgery + first two weeks post-surgery, Figure 5d, two-way repeated-measures ANOVA/Holm-Sidak, g1, $p=0.002$, g2, $p=0.03$). There was no difference in LH pulse frequency measured on the day of estrus or mean levels between Arc-AAV-*Esr1* vs Arc-AAV-*lacZ* injected mice on estrus (Figure 5c, e, f). Notably, LH response to kisspeptin and to GnRH was reduced in Arc-AAV-*Esr1* mice (Figure 5g, two-way repeated measures ANOVA/Holm-Sidak, *lacZ*, control vs kisspeptin or GnRH, $p<0.001$; *Esr1* vs *lacZ* for kisspeptin and GnRH both, $p\leq0.002$).

Knockdown of ERα in arcuate kisspeptin neurons in adulthood increase ionotropic glutamatergic transmission to these cells but does not alter their short-term spontaneous firing rate.

Arcuate kisspeptin neurons are postulated to form an interconnected network that is steroid sensitive and utilizes glutamatergic transmission at least in part for intranetwork communication (Qiu et al., 2016). We thus hypothesized that loss of ERα specifically from arcuate kisspeptin neurons would increase their spontaneous firing rate and increase glutamatergic transmission to these cells, similar to what is observed in these cells in KERKO mice(Wang et al., 2018). As Arc-AAV-*Esr1* knockdown mice spend most time in estrus, similar to KERKO mice, we used

estrus as the reproductive stage to examine the short-term (~10min) firing frequency of these neurons and AMPA-mediated excitatory glutamatergic postsynaptic currents (EPSCs). The firing frequency of Arc-AAV-*Esr1* infected cells was not different from Arc-AAV-*lacZ* infected cells (Figure 6a, b, Mann-Whitney U-test, p=0.14) even though there tends to be more cells firing at >1Hz in the Arc-AAV-*Esr1* group compared to the Arc-AAV-*lacZ* group (Figure 6c, Fisher's exact test, *Esr1* vs *lacZ*, p=0.07). In contrast, the frequency and amplitude of glutamatergic EPSCs in arcuate kisspeptin cells in Arc-AAV-*Esr1* infected mice was greater than in the Arc-AAV-*lacZ* group (Figure 6d, e, f, two-tailed unpaired Student's t-test, frequency p=0.0007, amplitude p=0.014).

Discussion

This study examined the roles of two hypothalamic kisspeptin neuronal populations in mediating estradiol feedback from cellular, molecular and whole-body physiology perspectives. We utilized both conventional kisspeptin-specific ERα knockout mice (KERKO) and CRISPR-Cas9 based viral vector-mediated knockdown of *Esr1*. The latter approach allows both temporal control and nucleus-specific manipulations to distinguish the role of ERα within each population in negative and positive feedback regulation of LH release and neurobiological properties (Figure 7).

AVPV kisspeptin neurons are postulated to convey estradiol positive feedback signals to generate the GnRH surge. Consistent with this postulate, these neurons are more excitable during positive feedback and also receive increased glutamatergic transmission (Piet et al., 2013; Zhang et al., 2013; Wang et al., 2016, 2018). AVPV kisspeptin cells in both KERKO and AVPV-AAV-*Esr1* models are less excitable compared to controls, firing fewer bursts and single action potentials in response to the same current injection. Results from the AVPV-AAV-*Esr1* model support and extend data from KERKO mice and provide evidence towards accepting the hypothesis that the role of ERα in shifting excitability is activational, independent of its role in the development of these cells (Mayer et al., 2010).

Kisspeptin expression in AVPV cells is estradiol activated and fewer cells expressing *Kiss1* mRNA are detected in this region in KERKO mice (Greenwald-Yarnell et al., 2016). In AVPV-AAV-*Esr1* mice with adult knockdown, we also observed fewer cells express *Kiss1* mRNA compared to AVPV-AAV-*lacZ* mice, further supporting an activational role for estradiol in the adult physiology of these cells. The inability to sense estradiol through ERα in AVPV kisspeptin neurons may reduce production and release of kisspeptin and ultimately impair the downstream GnRH/LH surge. This could explain the blunted LH surges in AAV-*Esr1* injected mice. *Esr1*

knockdown in AVPV, however, did not alter reproductive cyclicity monitored by changes in vaginal cytology. Vaginal cytology reflects circulating steroids, in particular estradiol. Of note, only some of these mice had evidence of typical ovulation monitored by the number of corpra lutea. It is possible that sufficient estradiol is produced during these cycles to induce vaginal cytology, but not to trigger an LH surge. It is important to point out, however, that estradiol-induced LH surges, in which an established dose of estradiol was provided to the mouse, were also blunted in AVPV-AAV-*Esr1* mice. This latter observation suggests that inappropriate response of the neuroendocrine system to estradiol is, at least in part, responsible for the blunting of the LH surge. With regard to the continuation of estrous cycles in the AVPV-AAV-*Esr1* mice, typical function of the remaining ERα-positive AVPV kisspeptin neurons may be sufficient to drive maintain cyclicity. Alternatively, cyclicity and the associated changes in sex steroids may be controlled by other cells that express ERα. Of interest, stress or neuronal androgen receptor KO can similarly disrupt the LH surge without a change in estrous cyclicity (Wagenmaker and Moenter, 2017; Walters et al., 2018).

In support of a non-AVPV kisspeptin neuronal population being a primary driver of estrous cyclicity, several reproductive phenotypes of KERKO and AVPV-targeted ERα knockdown mice are different. KERKO mice tend to exhibit prolonged vaginal cornification and enlarged uteri, neither of which were observed in mice in which AAV-*Esr1* infection was targeted to the AVPV (Figure 1- figure supplement 1c). In contrast, prolonged estrus and enlarged uteri were observed in mice in which Arc-AAV-*Esr1* infection was targeted to arcuate kisspeptin neurons. These latter neurons have been postulated to play a role in generating episodic GnRH output. Changes in episodic GnRH frequency drive gonadotropins and thus follicle development and steroidogenesis, including the estradiol rise, which triggers positive feedback and changes in vaginal cytology. Long-term firing output of arcuate kisspeptin neurons in brain slices is episodic and steroid modulated (Vanacker et al., 2017), and activation of these cells *in vivo* generates a pulse of LH release (Clarkson et al., 2017). Further evidence comes from *Tac2*-specific ERα KO mice, in which ERα is primarily deleted from the arcuate, not the AVPV, kisspeptin population. These mice also exhibit prolonged vaginal cornification (Greenwald-Yarnell et al., 2016). We thus hypothesize that ERα in arcuate kisspeptin neurons contributes to maintaining pulsatile LH release and mediates central estradiol negative feedback.

Consistent with this postulate, partial (~65%) adult knockdown of ERα in these cells altered the reproductive cycle. As KERKO mice exhibit increased LH-pulse frequency, we were initially surprised we did not observe differences in pulse frequency or mean LH levels in mice receiving

Arc-AAV-*Esr1*. This may be attributable to single hosing conditions in the present experiment, which may make mice prone to stress despite more than four weeks of handling before sampling. It is also possible that the pulse frequency during diestrus differs between Arc-AAV-*Esr1* and Arc-AAV-*lacZ* mice. Despite this lack of statistical difference in LH-pulse frequency, ERα knockdown mice had markedly reduced response to IP injection of both kisspeptin and GnRH, similar to KERKO mice (Wang et al., 2018). This suggests loss of ERα function in arcuate kisspeptin neurons may disrupt GnRH neuronal response to kisspeptin and/or the pituitary response to GnRH. This could arise from a disruption of negative feedback leading to overstimulation and thus desensitization of the hypothalamo-pituitary-gonadal axis or blunting of the response to administered neuropeptides.

Dissection of the electrophysiological properties of arcuate kisspeptin neurons revealed that glutamatergic transmission to these neurons was elevated when ERα is knocked down. This indicates the connectivity of these cells remains plastic even after puberty. The observation that targeted reduction of ERα in arcuate kisspeptin neurons increases glutamatergic transmission further suggests interconnections among these cells provide many of their glutamatergic inputs. Given this, it is intriguing that the short-term firing rate of these cells was not increased, although there was a strong trend towards a greater percent of higher-frequency cells. The lack of change in mean firing rate may reflect the partial deletion of ERα in this population, with lower firing rate being preserved in cells with ERα, and elevated EPSC frequency arising at least in part from the high firing cells. It is also possible that long-term firing patterns of these Arc-AAV-*Esr1* infected arcuate kisspeptin neurons, which may be associated with episodic neuroendocrine activity, are disrupted. These data support the idea that glutamatergic inputs to arcuate kisspeptin neurons play an important role on maintaining normal reproductive function.

Although the CRISPR-Cas9 based knockdown approach allows spatial and temporal control, it too has caveats. For example, sgRNAs may have off-target actions on other regions of the genome beyond the sites predicted by the design software (Anderson et al., 2018). To address this, we independently tested two sgRNAs that target *Esr1* to address the possible off-target effects among groups. We did not observe any differences between *Esr1* guide1 and guide2 groups. This suggests the phenotypes observed are primarily attributable to the deletion of ERα. Because of the nature of the nonhomologous end joining repair machinery activated after CRISPR-Cas9-initiated cuts, *Esr1* gene editing in each cell varies. It is difficult to assess each individual neuron to test if mutations at other genes are potentially involved in changes

biophysical properties. Despite these variables, in the present study the systemic and cellular phenotypes in *Esr1* guide1 vs guide2 infected mice were quite consistent.

In conclusion, utilizing CRISPR-Cas9 AAV, we were able to successfully knockdown ERα in specific populations of kisspeptin neurons in adult female mice. Knockdown in each population recapitulated part of the KERKO model and furthers our understanding the role ERα in that population in regulating estradiol feedback.

Materials and Methods

Key Resources Table

Reagent type (species) or resource	Designation	Source or reference	Identifiers	Additional information
strain, strain background (Mus musculus)	Kiss1-ires-Cre C57BL/6J mice	PMID 26862996		Dr. Martin Myers, University of Michigan
strain, strain background (Mus musculus)	Esr1 loxp C57BL/6J mice	PMID 17785410		Dr. Martin Myers, University of Michigan
strain, strain background (Mus musculus)	Cas9-stop loxp C57BL/6J mice	Jackson Labs	Jax 024858; RRID:IMSR_JAX:024858	
strain, strain background (Mus musculus)	Rosa26-EYFP C57BL/6J mice	Jackson Labs	Jax 006148; RRID:IMSR_JAX:006148	
cell line (Mus musculus)	C2C12 myoblast, C3H	ATTC	Cat # CRL 1772	Dr. Daniel Michele, University of Michigan
antibody	anti-ERα, polyclonal antibody, rabbit	Millipore	#06-935	dil. 1:10000, Immunogen, C-terminus of Estrogen Receptor alpha.
antibody	anti-mCherry, monoclonal antibody, rat	Invitrogen	M11217	dil. 1:5000. Immunogen, full-length protein mCherry
antibody	anti-GFP, polyclonal	Abcam	ab13970	dil. 1:2000. Immunogen, full

	antibody, chicken			length protein GFP
recombinant DNA reagent	AAV8-hsyn-dio-sgRNA_lacZ-mCherry	The sgRNA sequence is provided in the method section; the plasmid was packed to AAV8 in UNC vector core	Custom Order	Plasmid backbone was provided by Dr. Martin Myers, University of Michigan
recombinant DNA reagent	AAV8-hsyn-dio-sgRNAEsr1_g1-mCherry	The sgRNA sequence is provided in the method section; the plasmid was packed to AAV8 in UNC vector core	Custom Order	Plasmid backbone was provided by Dr. Martin Myers, University of Michigan
recombinant DNA reagent	AAV8-hsyn-dio-sgRNAEsr1_g2-mCherry	The sgRNA sequence is provided in the method section; the plasmid was packed to AAV8 in UNC vector core	Custom Order	Plasmid backbone was provided by Dr. Martin Myers, University of Michigan
recombinant DNA reagent	plasmid LentiV2-sgRNA-Esr1_g1	The sgRNA sequence is provided in the method section.	built on lentiCRISPR v2; Addgene Cat #52961	The plasmid backbone was provided by Dr. Yatrik Shah, University of Michigan
recombinant DNA reagent	plasmid LentiV2-sgRNA-Esr1_g2	The sgRNA sequence is provided in the method section.	built on lentiCRISPR v2; Addgene Cat #52961	The plasmid backbone was provided by Dr. Yatrik Shah, University of Michigan
recombinant DNA reagent	plasmid LentiV2-sgRNA-lacZ	The sgRNA sequence is provided in the method section.	built on lentiCRISPR v2; Addgene Cat #52961	The plasmid backbone was provided by Dr. Yatrik Shah, University of Michigan
commercial assay or kit	ABC amplification	Vector Laboratories	Cat # PK-6100	
chemical compound, drug	CNQX	Sigma-Aldrich	Cat # 1045	
chemical compound, drug	APV	Tocris	Cat # 0106	
chemical compound, drug	picrotoxin	Sigma-Aldrich	Cat # P1675	
chemical compound, drug	TTX	Tocris	Cat # 1069	
chemical	10% Neutral	Fisher Scientific	Cat #	

compound, drug	Buffered Formalin		22899402	
chemical compound, drug	Hydrogen Peroxide	Sigma	Cat # 216763	
chemical compound, drug	LHRH	Bachem	Cat # H4005	
chemical compound, drug	kisspeptin	Phoenix	Cat # 048-56	
chemical compound, drug	Neurobiotin	Vector Labs	Cat # SP-1120	
software, algorithm	Igor Pro	Wavemetrics	https://github.com/defazio2/LWeLifeRepo	

Chemicals were from Sigma Chemical Company unless noted.

Animals. The University of Michigan Institutional Animal Care and Use Committee approved all procedures. Adult female mice (60-150 days) were used. Mice were provided with water and Harlan 2916 chow (VetOne) *ad libitum* and were held on a 14L:10D light cycle (lights on 0400 Eastern Standard Time). To delete ERα specifically from kisspeptin cells (Wang et al., 2018), mice with the *Cre* recombinase gene knocked-in after the *Kiss1* promoter (*Kiss1*-Cre mice) were crossed with mice with a floxed *Esr1* gene, which encodes ERα (ERα floxed mice)(Greenwald-Yarnell et al., 2016). The expression of Cre recombinase mediates deletion of ERα in kisspeptin cells (KERKO mice). To visualize kisspeptin neurons for recording, mice heterozygous for both Kiss-Cre and floxed ERα were crossed with Cre-inducible YFP mice. Crossing mice heterozygous for all three alleles yielded litters that contained some mice that were homozygous for floxed ERα and at least heterozygous for both *Kiss1*-Cre and YFP; these were used as KERKO mice. Littermates of KERKO mice with wild type *Esr1, Kiss1*-Cre YFP (heterozygous or homozygous for either Cre or YFP) were used as controls; no differences were observed among these controls and they were combined.

To generate kisspeptin-specific S. pyogenes Cas9 (Cas9)-expressing mice, mice with the *Cre* recombinase gene knocked-in after the *Kiss1* promoter (*Kiss1-Cre* mice) were crossed with mice that have Cre recombinase-dependent expression of CRISPR-associated protein 9 (Cas9) endonuclease, a 3X-FLAG epitope tag and eGFP directed by a CAG promoter. KERKO mice have disrupted estrous cycles with persistently cornified vaginal cytology typical of estrus; we thus used females in estrus as controls. Estrous cycle stage was determined by vaginal lavage.

To examine the role of circulating estradiol, mice were ovariectomized (OVX) under isoflurane anesthesia (Abbott) and were either simultaneously implanted with a Silastic (Dow-Corning) capsule containing 0.625 µg of estradiol suspended in sesame oil (OVX+E) or not treated further (OVX)(Christian et al., 2005). Bupivacaine (0.25%, APP Pharmaceuticals) was provided local to incisions as an analgesic. These mice were studied 2-3d after surgery. Mice for electrophysiology were sacrificed at the time of estradiol positive feedback in the late afternoon (Christian et al., 2005). For free-floating immunochemistry staining, mice were perfused at 1700 EST 2-3d post OVX+E surgery at the expected peak of the estradiol-induced LH surge.

sgRNA design. For Cas9 target selection and generating single guide RNAs (sgRNA), 20-nt target sequences were selected to precede a 5'NGG protospacer-adjacent motif (PAM) sequence. To minimize off-targeting effects and maximize sgRNA activity, two CRISPR design tools were used to evaluate sgRNAs (Ran et al., 2013; Doench et al., 2014) targeting mouse *Esr1* exon1. The two best candidates were selected based on lowest predicted off-target effects and highest activity. The target sequence for guide 1 is 5'-CACTGTGTTCAACTACCCCG-3' (referred to as g1) and the target sequence for guide 2 is 3'-CTCGGGGTAGTTGAACACAG-5' (referred to as g2). Because g1 and g2 were similarly effective in *Esr1* knockdown and effects on cycles, mice were combined for physiology studies. Control sgRNA sequence was designed to target *lacZ* gene from *Escherichia coli* (target sequence: 5'-TGCGCAGCCTGAATGGCGAA -3').

In vitro validation of sgRNAs. Mycoplasma-free C2C12 mouse myoblast cells (generous gift of Dr. Daniel Michele, University of Michigan) were grown in DMEM containing 10% FBS (Thermo Fisher) at 37°C in 5% CO2. Each individual sgRNA was introduced to BsmBI site of the lentiCRISPRv2 construct. Cells were co-transfected with one of the lentiCRISPRv2 plasmids containing sgRNAs and a standard GFP plasmid construct (Ramakrishnan et al., 2016) using Lipofectamine 3000 (Invitrogen) according to the manufacturer's instructions. Cells were selected for ~4 weeks with medium containing 1 µg/mL puromycin. Selected cells were harvested, DNA isolated using the Qiagen DNA Extraction Kit, and sequenced with primers for *Esr1*.

AAV vector production. To construct the AAV plasmid, a mCherry-U6 promoter-sgRNA scaffold segment was synthesized by Integrated DNA Technologies (IDT). After PCR amplification, the ligation product containing mCherry-U6 promoter-sgRNA scaffold was cloned in reverse orientation into a hSyn (human Synapsin 1) promoter driven *Cre*-inducible AAV vector backbone (Flak et al., 2017). The individual sgRNAs (with an extra G added to the 5'-end of each sgRNA

to increase guide efficiency (Doench et al., 2014)) were then inserted into a designed SapI site between U6 promoter and sgRNA scaffold component. All three AAV viral vectors were prepared in AAV8 serotype at University of North Carolina Vector Core.

Stereotaxic injections. Kiss1Cre/Cas9-GFP female animals (>2 mo) were checked for estrous cycles for >10 days before surgery; only mice with regular 4-5 day cycles were used. Mice were anesthetized with 1.5%–2% isoflurane. AVPV injections were targeted to 0.55 mm posterior to Bregma, ±0.2mm lateral to midline, and 4.7 and 4.8mm ventral to dura. Arcuate injections were targeted to 1.5-1.7mm posterior to Bregma, ±0.2mm lateral to midline, and 5.9mm ventral to dura. 100nl virus injected bilaterally at the target coordinates at ~5nl/min. The pipette was left in place for 5 min after injection to allow viral diffusion into the brain. Carprofen (5 mg/kg, sc) was given before and 24h after surgery to alleviate postsurgical pain. Estrous cycle monitoring continued after surgery for up to eight weeks. Stereotaxic hits were defined as ≥70% infection rate in both hemispheres; only bilateral hits were included for *in vivo* evaluation of reproductive parameters.

Perfusion and free-floating immunohistochemistry. Mice were anesthetized with isoflurane and then transcardially perfused with PBS (15-20mL) then 10% neutral-buffered formalin for 10min (~50mL). Brains were placed into the same fixative overnight, followed by 30% sucrose for ≥24h for cryoprotection. Sections (30µm, 4 series) were cut on a cryostat (Leica CM3050S) and stored at -20°C in antifreeze solution (25% ethylene glycol, 25% glycerol in PBS). Sections were washed with PBS, treated with 0.1% hydrogen peroxide, and then placed in blocking solution (PBS containing 0.1% TritonX-100, 4% normal goat serum) for 1h at room temperature, then incubated with rabbit anti-ERα (#06-935, Millipore, 1:10,000; this antibody recognizes the C-terminus of ERα.) in blocking solution 48h at 4°C. Sections were washed then incubated with biotinylated anti-rabbit antibody (Jackson Immunoresearch, 1:500) followed by ABC amplification (Vector Laboratories, 1:500) and nickel-enhanced diaminobenzidine (Thermo Scientific) reaction (4.5min). Sections were washed with PBS and incubated overnight with chicken anti-GFP (ab13970, Abcam, 1:2000) and rat anti-mCherry (M11217, Invitrogen, 1:5000) in blocking solution. The next day, sections were washed and incubated with Alexa 594-conjugated anti-rat and Alexa 488-conjugated anti-chicken antibodies for 1h at room temperature (Molecular Probes, 1:500). Sections were mounted and coverslipped (VWR International 48393 251). Images were collected on a Zeiss AXIO Imager M2 microscope, and the number of immunoreactive GFP only, GFP/mCherry, and GFP/mCherry/ERα cells were

counted in the injected region. The other kisspeptin region in the hypothalamus was examined and no infection of kisspeptin cell bodies was observed.

Brain slice preparation All solutions were bubbled with 95%O_2 and 5%CO_2 for ≥15min before exposure to tissue and throughout experiments. Brains were rapidly removed 1.5-2h before lights off and placed in ice-cold sucrose saline solution containing (in mM): 250 sucrose, 3.5 KCl, 25 $NaHCO_3$, 10 D-glucose, 1.25 Na_2HPO_4, 1.2 $MgSO_4$, and 3.8 $MgCl_2$. Coronal slides (300μm) were made with a Leica VT1200S. Slices were incubated in a 1:1 mixture of sucrose-saline and artificial cerebrospinal fluid (ACSF) containing (in mM): 135 NaCl, 3.5 KCl, 26 $NaHCO_3$, 10 D-glucose, 1.25 Na_2HPO_4, 1.2 $MgSO_4$, 2.5 $CaCl_2$ for 30 min at room temperature. Slices were then transferred to 100% ACSF at room temperature for ≥30min before recording. Slices were used within 6h of preparation.

Electrophysiology recordings Slices were transferred to a recording chamber and perfused with oxygenated ACSF (3mL/min) and heated by an in-line heater (Warner Instruments) to 30±1 °C. GnRH-GFP neurons were identified by brief illumination at 470nm using an upright fluorescence microscope Olympus BX51W1. Recording pipettes were pulled from borosilicate glass (type 7052, 1.65mm outer diameter and 1.12mm inner diameter; World Precision Instruments, Inc.) using a P-97 puller (Sutter Instruments) to obtain pipettes with a resistance of 2-3.5MΩ. Recordings were performed with an EPC-10 dual-patch clamp amplifier and Patchmaster acquisition software (HEKA Elektronik). Recorded cells were mapped to a brain atlas (Paxinos and Franklin, 2001) to determine if cell location was related to response to treatment. No such correlation was observed in this study.

Extracellular recordings. Extracellular recordings were used to characterize firing rate as they maintain internal milieu and have minimal impact neuronal firing rate (Nunemaker et al., 2003; Alcami et al., 2012). Recordings were made with receptors for ionotropic $GABA_A$ and glutamate synaptic transmission antagonized (100μM picrotoxin, 20μM APV [D-(−)-2-amino-5-phosphonovaleric acid], 10μM CNQX [6-cyano-7-nitroquinoxaline]). Pipettes were filled with HEPES-buffered solution containing (in mM): 150 NaCl, 10 HEPES, 10 D-glucose, 2.5 $CaCl_2$, 1.3 MgCl2, and 3.5 KCl (pH=7.4, 310 mOsm), and low-resistance (22±3MΩ) seals formed between the pipette and neuron after first exposing the pipette to the slice tissue in the absence of positive pressure. Recordings were made in voltage-clamp mode (0mV pipette holding potential) and signals acquired at 20kHz and filtered at 10kHz. Resistance of the loose seal was checked frequently during the first 3min of recordings to ensure a stable baseline, and also

before and after a subsequent 10-min recording period; data were not use if seal resistance changed >30% or was >25MΩ. The first 5min of this 10-min recording were consistently stable among cells and were thus used for analysis.

Whole-cell recordings. For whole-cell patch-clamp recordings, three different pipette solutions were used depending on the goal. Most recordings were done with a physiologic pipette solution containing (in mM): 135 K gluconate, 10 KCl, 10 HEPES, 5 EGTA, 0.1 $CaCl_2$, 4 MgATP and 0.4 NaGTP, pH 7.2 with NaOH, 302±3 mOsm. A similar solution containing 10mM neurobiotin was adjusted to similar osmolarity. A solution in which cesium gluconate replaced potassium gluconate was used to reduce potassium currents and allow better isolation of calcium currents. Membrane potentials reported were corrected online for liquid junction potential of -15.7 mV, same among all solutions (Barry, 1994).

After achieving a minimum 1.6GΩ seal and the whole-cell configuration, membrane potential was held at -70mV between protocols during voltage-clamp recordings. Series resistance (R_s), input resistance (R_{in}), holding current (I_{hold}) and membrane capacitance (C_m) were frequently measured using a 5mV hyperpolarizing step from -70mV (mean of 16 repeats). Only recordings with R_{in} >500 MΩ, I_{hold} -40 to 10pA and R_S <20MΩ, and stable C_m were accepted. R_s was further evaluated for stability and any voltage-clamp recordings with ΔR_s >15% were excluded; current-clamp recordings with ΔR_s >20% were excluded. There was no difference in I_{hold}, C_m, or R_s among any comparisons.

For current-clamp recordings, depolarizing and hyperpolarizing current injections (-50 to +50pA, 500ms, 10pA increments) were applied from an initial membrane potential of -71±2 mV, near the resting membrane potential of these cells (DeFazio et al., 2014).

For voltage-clamp recordings of excitatory postsynaptic currents (EPSCs), membrane potential was held at -68mV, the reversal potential for $GABA_A$-receptor mediated currents, and ACSF contained picrotoxin (100μM), and APV (D-(−)-2-amino-5-phosphonovaleric acid, 20μM).

For voltage-clamp recordings of I_T, ACSF containing antagonists of ionotropic $GABA_A$ and glutamate receptors was supplemented with TTX (2μM) and the Cs-based pipette solution was used. Two voltage protocols were used to isolate I_T as reported (Wang et al., 2016). First, total calcium current activation was examined. Inactivation was removed by hyperpolarizing the membrane potential to −110mV for 350ms (not shown in figures). Next a 250ms prepulse of -110mV was given. Then membrane potential was varied in 10mV increments for 250ms from −110 to -30mV. Finally, test pulse of -40mV for 250ms was given. From examination of the

current during the test pulse, it was evident that no sustained (high-voltage activated) calcium current was activated at potentials more hyperpolarized than -40mV. To remove HVA contamination from the step to -30mV, a second protocol was used in which removal of inactivation (-110mV, 350ms) was followed by a 250ms prepulse at -40mV, then a step for 250ms at -30mV and finally a test pulse of -40mV for 250ms. I_T was isolated by subtracting the trace following the -40mV prepulse from those obtained after the -110mV prepulse for the depolarized variable step to -30mV; raw traces from the initial voltage protocol were used without subtraction for variable steps from -110mV to -40mV because of the lack of observed activation of HVA at these potentials. Activation of I_T was assessed from the resulting family of traces by peak current during the variable step phase. Inactivation of I_T was assessed from the peak current during the final -40mV test pulse.

Post hoc identification of ERα. The pipette solution containing neurobiotin was used for recordings cells from AAV-injected mice. An outside-out patch was formed after recording to reseal the membrane and the location of cells was marked on a brain atlas (Paxinos and Franklin, 2001). The brain slices were fixed overnight in 10% formalin at 4°C and changed to PBS. Slices were photo-bleached with a UV illuminator for ~72h and checked to ensure no visible fluorescent signal was observed. Slices were then placed in blocking solution for 1h, then incubated with rabbit anti-ERα for 48h at 4°C. Slices were washed and then incubated with Alexa 594-conjugated anti-rabbit and Alexa 350-conjugated neutravidin for 2h at room temperature (Molecular Probes, 1:500). Slices were mounted, coverslipped and imaged as above. Cells with neurobiotin-labeling were examined for ERα-immunoreactivity.

Single-cell PCR Cells for single cell PCR were collected as previously described(Ruka et al., 2013). Patch pipettes (2–3MΩ) were filled with 5–8μL of an RNase free solution containing (in mM) 135 K-gluconate, 10 KCl, 10 HEPES, 5 EGTA, 4.0 Mg-ATP, 0.4 Na-GTP, and 1.0 $CaCl_2$ (pH 7.3, 305 mOsm). Additionally, just before use 1U/μL Protector RNase Inhibitor (Roche, Indianapolis, IN) was added to the pipette solution. Single Cell RNA was harvested from the target cells in whole-cell configuration after recording membrane response in current-clamp; cytoplasm was aspirated into the pipette and expelled into a 0.2mL tube containing reverse transcriptase buffer (Superscript Vilo cDNA Synthesis Kit, Invitrogen/ThermoFisher), volume was adjusted to 20μL with molecular grade water. Cell contents were reverse transcribed following manufacture's instructions. False harvests, in which the pipette was lowered into the slice preparation but no aspiration of cell contents occurred, were used to estimate background contamination. These were performed on each recording day. Additionally, a standard curve of

mouse hypothalamic RNA (1, 0.1, 0.01, 0.001 ng/μL final concentration) and a water blank (negative control) were reverse transcribed. An equivalent volume of water or patch solution was reverse transcribed as a negative control. Single-cell cDNA, controls, and the standard curve were preamplified for 15 cycles using TaqMan PreAmp Master Mix (Invitrogen/ThermoFisher) as previously described (Glanowska et al., 2014). Quantitative PCR was performed using 5μL of diluted preamplified DNA (1:10) per reaction, in duplicate, for 50 cycles (TaqMan Gene Expression Master Mix; Invitrogen). Single cell cDNA was assayed for: Kiss1, TH, Esr1, Esr2, Pgr, Cacna1g, Cacna1h, Cacna1i, Hcn1 Hcn2 Hcn3 Hcn4; Syn1 was used as housekeeping gene; only Syn1 positive cells were analyzed. Single cells were considered positive for a transcript if their threshold was a minimum of three cycles earlier (8 fold greater) than the false harvests and the reverse transcribed and preamplified water blank sample. TaqMan PrimeTime qPCR assays for mRNAs (Table 4) were purchased from IDT.

Tail-tip blood collection for LH pulses. Ovary-intact Kiss1Cre-Cas9 adult female mice with AAV-*lacZ* and AAV-*Esr1* targeted to the arcuate nucleus were singly-housed were handled daily ≥4wks before sampling. Vaginal cytology of was determined for ≥10 days before sampling. As the majority of AAV-*Esr1* arcuate targeted mice (6 of 9) exhibit prolonged cornification typical of estrus, all mice (*Esr1* and *lacZ*) were sampled during estrus. Repetitive tail-tip blood collecting was performed as described (Steyn et al., 2013). After the excision of the very tip of the tail, blood (6μL) was collected every 6 min for 2h from 1pm to 3pm. At the end of this frequent sampling period, mice received a single intraperitoneal injection of kisspeptin (65μg/kg)(Hanchate et al., 2012). Blood was collected just before and 15 min after kisspeptin injection. GnRH (150μg/kg)(Glanowska et al., 2014) was injected 40-45 min after kisspeptin, with blood collected immediately before and 15 min after GnRH injection.

Tail-tip blood collection for LH surge Ovary-intact Kiss1Cre-Cas9 adult female mice with AAV-*lacZ* and AAV-*Esr1* targeted to the AVPV were singly-housed. Tail blood was collected as above on proestrus at 3, 4 and 5pm EST (lights are off at 5pm EST in the mouse room). One to two weeks later, these same mice were then subjected to OVX+E surgery and tail blood (6μL) was collected 2-3 days post-surgery at 9am and 5pm EST.

LH assay Whole blood was immediately diluted in 54μL of 0.1M PBS with 0.05% Tween 20 and 0.2%BSI, mixed and kept on ice. Samples were stored at −20 °C for a subsequent ultrasensitive LH assay (Steyn et al., 2013). Intraassay CV was 2.2%; interassay CVs were 7.3% (low QC, 0.13 ng/mL), 5.0% (medium QC, 0.8 ng/mL) and 6.5% (high QC, 2.3ng/mL). Functional sensitivity was 0.016ng/mL.

Ovarian histology Ovaries were fixed for 24h in 10% neutral-buffered formalin, then stored in 70% ethanol until paraffin embedding, sectioning (5µm) and H&E staining. Every fifth section was examined and *corpra lutea* counted.

Data analysis and statistics. Data were analyzed offline using custom software written in IgorPro 6.31 (Wavemetrics). For targeted extracellular recordings, mean firing rate in Hz was determined over 5 min of stable recording. In experiments examining I_T, the peak current amplitude at each step potential (V) was first converted to conductance using the calculated reversal potential of Ca^{2+} (E_{Ca}) and $G=I/(E_{Ca} - V)$, because driving force was linear over the range of voltages examined. The voltage dependencies of activation and steady-state inactivation were described with a single Boltzmann distribution: $G(V)= G_{max}/(1- \exp [(V_{1/2} - V_t)/k])$, where G_{max} is the maximal conductance, $V_{1/2}$ is the half-maximal voltage, and k is the slope. Current density of I_T at each tested membrane potential was determined by dividing peak current by membrane capacitance. LH pulses were detected by a version of Cluster (Veldhuis and Johnson, 1986) transferred to IgorPro using cluster sizes of two points for both peak and nadir and t-scores of two for detection of increases and decreases. Data were analyzed using Prism 7 (GraphPad Software) and reported as mean±SEM. The number of cells per group is indicated by n and the number of mice by N in Table 5. For two by two designs, data were normally distributed and analyzed by two-way ANOVA or two-way repeated-measures (RM) with Holm-Sidak *post hoc* analysis. For two group comparisons normally distributed data were analyzed by two-tailed unpaired Student's *t*-test; non-normal data were analyzed by Mann-Whitney U test. For categorical data, for more than 3 categories, *Chi*-square test of independence were used with Fisher's exact test as *post hoc* analysis. For two categories, Fisher's exact test was used. For each electrophysiological parameter comparison, no more than three cells per mouse was used in control and KERKO mice; no more than four cells per mouse was used for AAV-infected mice. No less than five mice were tested per parameter. The variance of the data was no smaller within an animal than among animals. For IHC staining, LH surge and LH pulse measurements, and reproductive cyclicity, at least three mice were tested per AAV vector.

Acknowledgements

We thank Elizabeth Wagenmaker for expert technical assistance. We thank Dr. Daniel Michele for sharing C2C12 cell lines with us. We thank University of Virginia Ligand Core for performing the ultra-sensitive LH assay.

Author contributions

LW: conceived and designed the work; acquired, analyzed and interpreted data; drafted the work

CV: acquired and interpreted data

LB: acquired and interpreted data, drafted the work

TB: acquired and interpreted data

YS: acquired and interpreted data

MGM: conceived of the work

SMM: conceived and designed the work; analyzed and interpreted data; drafted and edited the work

References

Alcami P, Franconville R, Llano I, Marty A (2012) Measuring the firing rate of high-resistance neurons with cell-attached recording. J Neurosci 32:3118–3130.

Anderson KR et al. (2018) CRISPR off-target analysis in genetically engineered rats and mice. Nat Methods 15:512–514.

Barry PH (1994) JPCalc, a software package for calculating liquid junction potential corrections in patch-clamp, intracellular, epithelial and bilayer measurements and for correcting junction potential measurements. J Neurosci Methods 51:107–116.

Cheong RY, Czieselsky K, Porteous R, Herbison AE (2015) Expression of ESR1 in glutamatergic and GABAergic neurons is essential for normal puberty onset, estrogen feedback, and fertility in female mice. J Neurosci 35:14533–14543.

Christian CA, Glidewell-Kenney C, Jameson JL, Moenter SM (2008) Classical estrogen receptor α signaling mediates negative and positive feedback on gonadotropin-releasing hormone neuron firing. Endocrinology 149:5328–5334.

Christian CA, Mobley JL, Moenter SM (2005) Diurnal and estradiol-dependent changes in gonadotropin-releasing hormone neuron firing activity. Proc Natl Acad Sci U S A 102:15682–15687.

Christian CA, Moenter SM (2010) The neurobiology of preovulatory and estradiol-induced gonadotropin-releasing hormone surges. Endocr Rev 31:544–577.

Clarkson J, Han SY, Piet R, McLennan T, Kane GM, Ng J, Porteous RW, Kim JS, Colledge WH, Iremonger KJ, Herbison AE (2017) Definition of the hypothalamic GnRH pulse generator in mice. Proc Natl Acad Sci 114:E10216–E10223.

Couse JF, Curtis SW, Washburn TF, Lindzey J, Golding TS, Lubahn DB, Smithies O, Korach KS (1995) Analysis of transcription and estrogen insensitivity in the female mouse after targeted disruption of the estrogen receptor gene. Mol Endocrinol 9:1441–1454.

DeFazio RA, Elias CF, Moenter SM (2014) GABAergic transmission to kisspeptin neurons is differentially regulated by time of day and estradiol in female mice. J Neurosci 34:16296–16308.

Docke F and Dörner G (1965) The mechanism of the induction of ovulation by estrogens. J Endocrinol 33:491-499.

Doench JG, Hartenian E, Graham DB, Tothova Z, Hegde M, Smith I, Sullender M, Ebert BL, Xavier RJ, Root DE (2014) Rational design of highly active sgRNAs for CRISPR-Cas9–mediated gene inactivation. Nat Biotechnol 32:1262–1267.

Dubois SL, Acosta-Martínez M, DeJoseph MR, Wolfe A, Radovick S, Boehm U, Urban JH,

631 Levine JE (2015) Positive, but not negative feedback actions of estradiol in adult female
632 mice require estrogen receptor α in kisspeptin neurons. Endocrinology:156(3):1111-20.
633 Flak JN, Arble D, Pan W, Patterson C, Lanigan T, Goforth PB, Sacksner J, Joosten M, Morgan
634 DA, Allison MB, Hayes J, Feldman E, Seeley RJ, Olson DP, Rahmouni K, Myers MG
635 (2017) A leptin-regulated circuit controls glucose mobilization during noxious stimuli. J Clin
636 Invest 127:3103–3113.
637 Glanowska KM, Burger LL, Moenter SM (2014) Development of Gonadotropin-releasing
638 hormone secretion and pituitary response. J Neurosci 34.
639 Glanowska KM, Venton BJ, Moenter SM (2012) Fast scan cyclic voltammetry as a novel
640 method for detection of real-time gonadotropin-releasing hormone release in mouse brain
641 slices. J Neurosci 32:14664–14669.
642 Greenwald-Yarnell ML, Marsh C, Allison MB, Patterson CM, Kasper C, MacKenzie A, Cravo R,
643 Elias CF, Moenter SM, Myers MG (2016) ERα in Tac2 neurons regulates puberty onset in
644 female mice. Endocrinology 157:1555–1565.
645 Han S, Gottsch ML, Lee KJ, Popa SM, Smith JT, Jakawich SK, Clifton DK, Steiner RA,
646 Herbison AE (2005) Activation of gonadotropin-releasing hormone neurons by kisspeptin
647 as a neuroendocrine switch for the onset of puberty. J Neurosci 25:11349–11356.
648 Hanchate NK, Parkash J, Bellefontaine N, Mazur D, Colledge WH, d'Anglemont de Tassigny X,
649 Prevot V (2012) Kisspeptin-GPR54 signaling in mouse NO-synthesizing neurons
650 participates in the hypothalamic control of ovulation. J Neurosci 32.
651 Helm KD, Nass RM, Evans WS, Nass RM, Evans WS (2009) Physiologic and pathophysiologic
652 alterations of the neuroendocrine components of the reproductive axis. In: Yen & Jaffe's
653 Reproductive Endocrinology, pp 441–488. Elsevier.
654 Hilton HN, Graham JD, Clarke CL (2015) Minireview: progesterone regulation of proliferation in
655 the normal human breast and in breast cancer: a tale of two scenarios? Mol Endocrinol
656 29:1230–1242.
657 Hrabovszky E, Steinhauser A, Barabás K, Shughrue PJ, Petersen SL, Merchenthaler I, Liposits
658 Z (2001) Estrogen receptor-beta immunoreactivity in luteinizing hormone-releasing
659 hormone neurons of the rat brain. Endocrinology 142:3261–3264.
660 Krege JH, Hodgin JB, Couse JF, Enmark E, Warner M, Mahler JF, Sar M, Korach KS,
661 Gustafsson JA, Smithies O (1998) Generation and reproductive phenotypes of mice
662 lacking estrogen receptor beta. Proc Natl Acad Sci U S A 95:15677–15682.
663 Kumar D, Candlish M, Periasamy V, Avcu N, Mayer C&, Boehm U (2015) Specialized
664 subpopulations of kisspeptin neurons communicate with GnRH neurons in female mice.

665 Endocrinology 156:32–38.
666 Kumar D, Freese M, Drexler D, Hermans-Borgmeyer I, Marquardt A, Boehm U (2014) Murine
667 arcuate nucleus kisspeptin neurons communicate with GnRH neurons in utero. J Neurosci
668 34.
669 Lee JH, Gomora JC, Cribbs LL, Perez-Reyes E (1999) Nickel block of three cloned T-type
670 calcium channels: low concentrations selectively block alpha1H. Biophys J 77:3034–3042.
671 Lehman MN, Coolen LM, Goodman RL (2010) Minireview: Kisspeptin/neurokinin B/dynorphin
672 (KNDy) cells of the arcuate nucleus: a central node in the control of gonadotropin-releasing
673 hormone secretion. Endocrinology 151:3479–3489.
674 Lubahn DB, Moyer JS, Golding TS, Couse JF, Korach KS, Smithies O (1993) Alteration of
675 reproductive function but not prenatal sexual development after insertional disruption of the
676 mouse estrogen receptor gene. Proc Natl Acad Sci U S A 90:11162–11166.
677 Macaluso M, Wright-Schnapp TJ, Chandra A, Johnson R, Satterwhite CL, Pulver A, Berman
678 SM, Wang RY, Farr SL, Pollack LA (2010) A public health focus on infertility prevention,
679 detection, and management. Fertil Steril 93:16.e1-10.
680 Mayer C, Acosta-Martinez M, Dubois SL, Wolfe A, Radovick S, Boehm U, Levine JE (2010)
681 Timing and completion of puberty in female mice depend on estrogen receptor alpha-
682 signaling in kisspeptin neurons. Proc Natl Acad Sci U S A 107:22693–22698.
683 Messager S, Chatzidaki EE, Ma D, Hendrick AG, Zahn D, Dixon J, Thresher RR, Malinge I,
684 Lomet D, Carlton MBL, Colledge WH, Caraty A, Aparicio SAJR (2005) Kisspeptin directly
685 stimulates gonadotropin-releasing hormone release via G protein-coupled receptor 54.
686 Proc Natl Acad Sci U S A 102:1761–1766.
687 Milanesi L, de Boland AR, Boland R (2008) Expression and localization of estrogen receptor α
688 in the C2C12 murine skeletal muscle cell line. J Cell Biochem 104:1254–1273.
689 Moenter SM, Caraty A, Karsch FJ (1990) The estradiol-induced surge of gonadotropin-releasing
690 hormone in the ewe. Endocrinology 127:1375–1384.
691 Nunemaker CS, DeFazio RA, Moenter SM (2003) A targeted extracellular approach for
692 recording long-term firing patterns of excitable cells: a practical guide. Biol Proced Online
693 5:53–62.
694 Oakley AE, Clifton DK, Steiner RA (2009) Kisspeptin signaling in the brain. Endocr Rev 30:713–
695 743.
696 Paxinos G, Franklin K (2001) The Mouse Brain in Stereotaxic Coordinates: Second Edition. San
697 Diego, CA: Elsevier Academic Press.
698 Pielecka-Fortuna J, Chu Z, Moenter SM (2008) Kisspeptin acts directly and indirectly to

699 increase gonadotropin-releasing hormone neuron activity and its effects are modulated by
700 estradiol. Endocrinology 149:1979–1986.
701 Piet R, Boehm U, Herbison AE, Zhang C, Tonsfeldt KJ, Qiu J, Bosch MA, Kobayashi K, Steiner
702 RA, Kelly MJ, Rønnekleiv OK (2013) Estrous cycle plasticity in the hyperpolarization-
703 activated current Ih Is mediated by circulating 17 -estradiol in preoptic area kisspeptin
704 neurons. J Neurosci 33:10828–10839.
705 Plant TM, Zeleznik AJ (2015) Knobil and Neill's physiology of reproduction 4th edition,
706 4thEdition ed. Elsevier.
707 Qiu J, Nestor CC, Zhang C, Padilla SL, Palmiter RD, Kelly MJ, Rønnekleiv OK (2016) High-
708 frequency stimulation-induced peptide release synchronizes arcuate kisspeptin neurons
709 and excites GnRH neurons. Elife 5:e16246.
710 Ramakrishnan SK, Zhang H, Takahashi S, Centofanti B, Periyasamy S, Weisz K, Chen Z, Uhler
711 MD, Rui L, Gonzalez FJ, Shah YM (2016) HIF2α is an essential molecular brake for
712 postprandial hepatic glucagon response independent of insulin signaling. Cell Metab
713 23:505–516.
714 Ran FA, Hsu PD, Wright J, Agarwala V, Scott DA, Zhang F (2013) Genome engineering using
715 the CRISPR-Cas9 system. Nat Protoc 8:2281–2308.
716 Ruka KA, Burger LL, Moenter SM (2013) Regulation of arcuate neurons coexpressing
717 kisspeptin, neurokinin B, and dynorphin by modulators of neurokinin 3 and κ-opioid
718 receptors in adult male mice. Endocrinology 154:2761–2771.
719 Sanjana NE, Shalem O, Zhang F (2014) Improved vectors and genome-wide libraries for
720 CRISPR screening. Nat Methods 11:783–784.
721 Semaan SJ, Murray EK, Poling MC, Dhamija S, Forger NG, Kauffman AS (2010) BAX-
722 dependent and BAX-independent regulation of Kiss1 neuron development in mice.
723 Endocrinology 151:5807–5817.
724 Smith JT, Cunningham MJ, Rissman EF, Clifton DK, Steiner RA (2005) Regulation of Kiss1
725 gene expression in the brain of the female mouse. Endocrinology 146:3686–3692.
726 Steyn FJ, Wan Y, Clarkson J, Veldhuis JD, Herbison AE, Chen C (2013) Development of a
727 methodology for and assessment of pulsatile luteinizing hormone secretion in juvenile and
728 adult male mice. Endocrinology 154:4939–4945.
729 Swiech L, Heidenreich M, Banerjee A, Habib N, Li Y, Trombetta J, Sur M, Zhang F (2014) In
730 vivo interrogation of gene function in the mammalian brain using CRISPR-Cas9. Nat
731 Biotechnol 33:102–106.
732 Vanacker C, Moya MR, DeFazio RA, Johnson ML, Moenter SM (2017) Long-term recordings of

arcuate nucleus kisspeptin neurons reveal patterned activity that is modulated by gonadal steroids in male mice. Endocrinology.

Veldhuis JD, Johnson ML (1986) Cluster analysis: a simple, versatile, and robust algorithm for endocrine pulse detection. Am J Physiol 250:E486-93.

Wagenmaker ER, Moenter SM (2017) Exposure to acute psychosocial stress disrupts the luteinizing hormone surge independent of estrous cycle alterations in female mice. Endocrinology 158:2593–2602.

Walters KA, Edwards MC, Tesic D, Caldwell ASL, Jimenez M, Smith JT, Handelsman DJ (2018) The role of central androgen receptor actions in regulating the hypothalamic-pituitary-ovarian axis. Neuroendocrinology 106:389–400.

Wang L, Burger LL, Greenwald-Yarnell ML, Myers MG, Moenter SM (2018) Glutamatergic transmission to hypothalamic kisspeptin neurons is differentially regulated by estradiol through estrogen receptor α in adult female mice. J Neurosci 38:1061 LP-1072.

Wang L, DeFazio RA, Moenter SM (2016) Excitability and burst generation of AVPV kisspeptin neurons are regulated by the estrous cycle via multiple conductances modulated by estradiol action. eNeuro 3:e0094-16.

Wintermantel TM, Campbell RE, Porteous R, Bock D, Gröne H-J, Todman MG, Korach KS, Greiner E, Pérez CA, Schütz G, Herbison AE (2006) Definition of estrogen receptor pathway critical for estrogen positive feedback to gonadotropin-releasing hormone neurons and fertility. Neuron 52:271–280.

Yip SH, Boehm U, Herbison AE, Campbell RE (2015) Conditional viral tract tracing delineates the projections of the distinct kisspeptin neuron populations to gonadotropin-releasing hormone (GnRH) neurons in the mouse. Endocrinology 156:2582–2594.

Zhang C, Tonsfeldt KJ, Qiu J, Bosch MA, Kobayashi K, Steiner RA, Kelly MJ, Rønnekleiv OK (2013) Molecular mechanisms that drive estradiol-dependent burst firing of Kiss1 neurons in the rostral periventricular preoptic area. Am J Physiol Endocrinol Metab 305:E1384-97.

Tables

Table 1. Statistical parameters for two-way ANOVA.

Parameter	Figure	Factor 1	Factor 2	Interaction
firing frequency	Figure1b	steroid F (2, 57) = 14.7 *	genotype F (1, 57) = 40.1 *	 F (2, 57) = 6.2 *
Input-output curve	Figure 1f intact OVX OVX+E	current F (4, 80) = 242.7 * F (4, 72) = 138.6 * F (4, 84) = 182.2 *	genotype F (1, 20) = 8.2 * F (1, 18) = 0.8 F (1, 21) = 6.6 *	 F (4, 80) = 0.6 F (4, 72) = 0.7 F (4, 84) = 1.5
I_T current density	Figure 2b	voltage F (8, 104) = 39.74 *	genotype F (1, 13) = 11.1 *	 F (8, 104) = 9.4 *
I_T normalized conductance	Figure 2c activation inactivation	voltage F (8, 104) = 494.7 * F (8, 104) = 195.8 *	genotype F (1, 13) = 3.2 F (1, 13) = 4.5 *	 F (8, 104) = 1.5 F (8, 104) = 3.1 *
LH	 Figure 3f Figure 3g	AAV type F (1, 12) = 29.8 * F (1, 13) = 0.3	time F (2, 24) = 2.1 F (1, 13) = 35.8 *	 F (2, 24) = 1.8 F (1, 13) = 19.5 *
input-output curve	Figure 4d IF post hoc PCR post hoc AAV-*Esr1* vs KERKO	current F (4, 136) = 165.5 * F (4, 68) = 123 * F (4, 100) = 154.7 *	AAV type F (2, 34) = 7.2 * F (1, 17) = 12.5 * F (1, 25) = 2.1	 F (8, 136) = 0.7 F (4, 68) = 4.3* F (4, 100) = 7.2
days proestrus /week	 Figure 5d	time F (1, 12) = 13.6 *	AAV type F (2, 12) = 5.8 *	 F (2, 12) = 10.0 *
LH	Figure 5g kisspeptin GnRH	injection F (1, 12) = 34.8 * F (1, 12) = 20.0 *	AAV type F (1, 12) = 4.7 # F (1, 12) = 7.0 *	 F (1, 12) = 17.1 * F (1, 12) = 7.5 *
		steroids	genotype	interaction
input resistance	Figure 1-figure supplement 1a	F (2, 59) = 2.6	F (1, 59) = 13.2 *	F (2, 59) = 2.0
cell capacitance	Figure 1-figure supplement 1b	F (2, 59) = 5.2	F (1, 59) = 0.1 *	F (2, 59) = 0.4
normalized uterine mass	Figure 1-figure supplement 1c	F (2, 30) = 19.9 *	F (1, 30) = 80.0 *	F (2, 30) = 2.4

* p<0.05, # p=0.05

Table 2. Statistical parameters for two group comparisons. For normally-distributed data, two-tailed unpaired Student's t-test, for non-normally distributed data, two-tailed Mann-Whitney U test.

Parameter	Figure	T or U, df
$V_{1/2}$ activation	in the text	t=1.7, 13
slope	control vs KERKO	t=0.01, 13
$V_{1/2}$ inactivation	I_T kinetics	t=2.5, 13
slope inactivation		t=1.6, 13
rate of rise IF	Figure 4h	t=2.5, 27
rate of rise PCR		t=2.7, 17
FWHM IF	Figure 4i	U=62
FWHM PCR		t=3.1, 17
AHP amplitude IF	Figure 4j	t=4.4, 27
AHP amplitude PCR		t=2.7, 27
LH pulses/h	Figure 5e	t=1.7, 12
mean LH	Figure 5f	t=0.05, 12
firing rate	Figure 6b	U=45.5
EPSC frequency	Figure 6e	t=4.0, 20
EPSC amplitude	Figure 6e	t=2.7, 20
input resistance	Figure 1-figure supplement 1a	
lacZ vs Esr1 IF		t=0.7, 27
lacZ vs Esr1 PCR		t=1.0, 17
KERKO vs Esr1		t=1.8, 35
cell capacitance	Figure 1-figure supplement 1b	
lacZ vs Esr1 IF		t=0.4, 27
lacZ vs Esr1 PCR		t=0.3, 17
KERKO vs Esr1		t=0.3, 35
normalized uterine mass	Figure 1-figure supplement 1c	
lacZ vs Esr1 AVPV		t=0.5, 14
lacZ vs Esr1 arcuate		t=2.9, 8

* p<0.05, # p=0.05

Table 3. Specificity of the *Esr1* sgRNAs and off-target predictions by Feng Zhang's guide design tool software (http://crispr.mit.edu); Benchling analysis (https://benchling.com/academic) produced a subset of these results.

sgRNA	* specificity score	& Mismatches (MMs) between sgRNA and gene locus	Gene		# Off-target score	Locus
Esr1-g1	90	4MMs [2:9:11:12]	NM_013870	*Smtn*	0.2	chr11:+3417882
		4MMs [5:10:13:19]	NM_009728	*Atp10a*	0.2	chr7:-66040030
		4MMs [4:9:15:20]	NM_023805	*Slc38a3*	0.1	chr9:+107561207
		4MMs [7:8:15:19]	NM_001037764	*Rai1*	0.1	chr11:+60003351
		4MMs [3:10:13:14]	NM_053193	*Cpsf1*	0.1	chr15:-76426196
Esr1-g2	73	4MMs [4:8:11:12]	NM_001024560	*Snx32*	0.4	chr19:+5495979
		4MMs [2:4:5:16]	NM_001194923	*Cldn18*	0.3	chr9:+99617489

*Values range from 1 to 100 index to assess the specificity of a guide, with 100 being the most specific guide.

& 4MMs [2:9:11:12] indicates nucleotides 2, 9, 11, 12 of the sgRNA do not match the 'off target' gene locus.

Off-target score values range from 0 to 100, with 100 being the value for the target *Esr1* gene.

781 **Table 4.** Primer probes used for single-cell qPCR

IDT Prime Time qPCR Probe Assay	Transcript	Forward 5'-3'	Reverse 5'-3'	Probe 5'-3'	amplicon (bp)	accession no.	Location
Mm.PT.58.42702897	*Cacna1g*	CTCAACTGTATCACCATCGCTA	AAGACTGCCGTGAAGATGT	CGCCCCAAAATTGACCCCCAC	101	NM_009783	4446-4546
Mm.PT.58.15908160	*Cacna1h*	GACACTGTGGTTCAAGCTCT	TTATCCTCGCTGCATTCTAGC	ACCTTGGTCTTCTTTTCATGCTCCTGT	122	NM_021415	5565-5686
Mm.PT.58.9567566	*Cacna1i*	CATCACCTTCATCATCTGCCT	CCTCCAGCACAAAGACAGT	ACCAGCCTACATCCCTAGAGACAGC	125	NM_001044308	4914-5038
Mm.PT.58.41764708	*Esr1*	GCTCCTTCTCATTCTTTCCCA	TCCAGGAGCAGGTCATAGAG	CCATGCCTTTGTTACTCATGTGCCG	108	NM_007956	1768-1865
Mm.PT.58.16981577	*Esr2*	CCTCCTGATGCTTCTTTCTCAT	TCGAAGCGTGTGAGCATTC	TCCATGCCCTTGTTACTGATGTGCC	133	NM_207707	1829-1961
Mm.PT.58.30501833	*Hcn1*	GCGTTATCACCAAGTCCAGTA	CAGTAGGTATCAGCTCGGACA	CTCCGAAGTAAGAGCCATCTGTCAGC	115	NM_010408	1913-2027
Mm.PT.58.7963736	*Hcn2*	CTTCACCAAGATCCTCAGTCTG	GGTCGTAGGTCATGTGGAAA	TGCGGCTATCACGGCTCATCC	98	NM_008226	935-1032
Mm.PT.58.7999585	*Hcn3*	GCCTCACTGATGGATCCTACT	TCAAGCACCGCATTGAAGT	ACCTATTGTCGCCTCTACTCGCTCA	130	NM_008227	1546-1675
Mm.PT.58.43863085	*Hcn4*	GCTGATGGCTCCTATTTTGGA	TCATTGAAGTTGTCCACGCT	AAGTATCCGCTCTGACGCTGGC	116	NM_001081192	2614-2729
Mm.PT.45.16269514	*Kiss1*	CTGCTTCTCCTCTGTGTCG	TTCCCAGGCATTAACGAGTTC.	CGGACTGCTGGCCTGTGGAT	105	NM_178260	66-170
Mm.PT.47.10254276	*Pgr*	CGCCATACCTTAACTACCTGAG	CCATAGTGACAGCCAGATGC	AGATTCAGAAGCCAGCCAGAGCC	124	NM_008829	2230-2353
Mm.PT.51.17048009.g	*Syn1*	CTTGAGCAGATT GCCATGTC	ACCTCAATAATGTGATCCCTTCC	ACGTGTCTACCCACAACTTGTACCTG	131	NM_013680	1159-1289
Mm.PT.58.33106186	*Th*	CCCTACCAAGATCAAACCTACC	CTGGATACGAGAGGCATAGTTC	TGAAGCTCTCTGACACGAAGTACACCG	96	NM_009377	1298-1393

782

783

Table 5. Number of cells (n) and number of mice (N) in each experiment. For AAV-injected mice, only animals with bilateral hits are included.

Figure 1a, b	Control	KERKO	
	Intact n=12, N=7	Intact n=11, N=6	
	OVX n=10, N=5	OVX n=11, N=4	
	OVX+E n=10, N=6	OVX+E n=9, N=5	
Figure 1c-f, Figure1-figure supplement 1a left, 1b left	Control	KERKO	
	Intact n=11, N=4	Intact n=11, N=5	
	OVX n=11, N=5	OVX n=9, N=4	
	OVX+E n=11, N=7	OVX+E n=12, N=5	
Figure 2	Control	KERKO	
	n=8, N=4	n=7, N=4	
Figure 3d,e	AVPV-AAV-*lacZ*	AVPV-AAV-*Esr1*g1	AVPV-AAV-*Esr1*g2
	N=3	N=3	N=4
Figure 3f	AVPV-AAV- *lacZ*	AVPV-AAV-*Esr1*	
	N=6	N= 8 (g1 N=4, g2 N=4)	
Figure 3g	AVPV-AAV- *lacZ*	AVPV-AAV-*Esr1*	
	N=6	N= 9 (g1 N=5, g2 N=4)	
Figure 4d-j and Figure 1-figure supplement 1 a middle, 1b middle	IF *post hoc*	PCR *post hoc*	
	Esr1 n=15, N=5	*Esr1* n=10, N=4	
	lacZ n=14, N=4	*lacZ* n=9, N=3	
	uninfected n=8, N=4	uninfected n=4, N=2	
Figure 5a-d	Arc-AAV-*lacZ*	Arc-AAV-*Esr1*g1	Arc-AAV-*Esr1*g2
	N=6	N=4	N=4
Figure 5e-g	Arc-AAV-*lacZ*	Arc-AAV-*Esr1*	
	N=6	N=8 (g1 N=4, g2 N=4)	
Figure 6a-c	Arc-AAV-*lacZ*	Arc-AAV-*Esr1*	
	n=11, N=5	n=13, N=5	
Figure 6d-f	Arc-AAV-*lacZ*	Arc-AAV- *Esr1*	
	n=10, N=5	n=12, N=5	
Figure 1-figure supplement 1a left, 1b right	KERKO	AVPV-AAV-*Esr1*	
	n=12, N=5	n=25, N=9	
Figure 1-figure supplement 1c left	Control	KERKO	
	Intact N=6	Intact n=11, N=7	
	OVX N=6	OVX n=11, N=6	
	OVX+E N=5	OVX+E n=9, N=7	
Figure 1-figure supplement 1c middle	AVPV-AAV-*lacZ*	AVPV-AAV-*Esr1*	
	N=7	N=9	
Figure 1-figure supplement 1c middle	Arc-AAV-*lacZ*	Arc-AAV-*Esr1*	
	N=5	N=5	
Figure 4-figure supplement 1	AVPV-AAV-*lacZ*	AVPV-AAV-*Esr1*	
	n=16, N=5	n=23, N=5 (g1 N=3, g2 N=2)	

Figure Legends

Figure 1 AVPV kisspeptin neurons from KERKO mice are less excitable compared to those from control mice and are not regulated by estradiol. **a**, representative extracellular recordings for cells from control and KERKO mice from ovary-intact, OVX and OVX+E groups. **b**, individual values and mean±SEM firing frequency of cells from control (white circles) and KERKO groups (black circles). **c**, representative depolarizing (magenta, +20pA, 500ms) and hyperpolarizing (black, -20pA, 500ms) firing signatures for cells from control and KERKO mice in ovary-intact (left), OVX (middle) and OVX+E (right) groups; black arrows indicate rebound bursts and red arrows indicate depolarization-induced bursts (DIB). Initial membrane potential was 70±2mV. **d** and **e**, percent of cells exhibiting DIB (**d**) or rebound (**e**) bursts; cells per group is shown within the bar. **f**, input-output curves for cells from control and KERKO mice; ovary-intact (left), OVX (middle) and OVX+E (right). * $p<0.05$

Figure 2. T-type calcium currents are reduced in AVPV kisspeptin neurons from KERKO compared to control mice. **a**, voltage protocol (bottom right) and representative I_T in control (left,) and KERKO groups (right). **b**, mean±SEM I_T current density in control (white symbols) and KERKO groups (black symbols). **c**, voltage dependence of I_T conductance activation and inactivation in cells from control and KERKO mice. * $p<0.05$.

Figure 3 *In vitro* and *in vivo* validation of AVPV-AAV-*Esr1* guides. **a**, sequencing from C2C12 cells transiently transfected with lentiCRISPR v2 with sgRNAs targeting *Esr1* (guide 1 [g1] top, guide 2 [g2] middle) or lacZ. N in yellow highlight indicates peak on peak mutations. **b** and **c**, Schematic representation of **b**, the Cre-inducible AAV vector delivering sgRNAs and **c**,*Kiss1*-cre *Cas9-loxp Stop-Gfp* mice. **d,** AVPV-AAV-*lacZ*, -*Esr1* g1 or g2 were bilaterally delivered to the AVPV region (see Figure 3- figure supplement 1). Brain sections were processed to detect GFP (green), mCherry (red) and ERα (black), dual GFP/mCherry detection indicates infection of kisspeptin neuron (white arrows, left panel of each pair). AVPV-AAV-*Esr1* infected AVPV kisspeptin neurons exhibit decreased ERα expression compared to AVPV-AAV-*lacZ* infected cells (right panel of each pair, white arrows indicate ERα-negative, magenta arrows indicate ERα-positive infected cells). **e**, representative reproductive cycles of mice that received AAV-*lacZ, g1 or g2*; E, estrus, D, diestrus, P proestrus, day 0 is the day of stereotaxic surgery. **f**, mean±SEM proestrous LH surge measured at 3, 4, and 5 pm EST in AVPV-AAV-*lacZ* and AVPV-AAV-*Esr1* mice (mice receiving g1 or g2 combined). **g,** mean±SEM estradiol-induced LH surge measured at 9 am and 5 pm EST from AAV-*lacZ* and AAV-*Esr1* OVX+E mice (mice receiving g1 or g2 were combined).

Figure 4 Decreased excitability of AVPV kisspeptin neurons in AVPV-AAV-*Esr1* knockdown mice. **a-c**, whole-cell recording and immunofluorescence (IF) *post hoc* identification of ERα in recorded cells in OVX+E AVPV-AAV-*Esr1* infected mice. **a**, visualization during recording; **b,** representative depolarizing (+20pA, magenta) and hyperpolarizing (-20pA, black) firing signatures. **c**, neurobiotin (blue) and ERα (red) staining after photobleaching of GFP and mCherry signals. From top to bottom: cells not infected by AVPV-AAV-*Esr1* and immunopositive for ERα; cells infected by AVPV-AAV-*Esr1* but still immunopositive for ERα; cells infected by AAV-*Esr1* and not immunopositive for ERα; cells infected by AVPV-AAV-*LacZ* and immunopositive for ERα. **d**, left, input-output curves of infected cells with undetectable ERα in AAV-*Esr1* (third row in a-c, black circle), cells infected by *AVPV*-AAV-*lacZ* (bottom row in a-c, orange circle, n=14), and cells not infected by AAV (top row in a-c, white circle); middle, input-output curves from a separate set of cells in which *Esr1* status was confirmed by single-cell qPCR *post hoc* (AAV-*Esr1* black circle, AAV-l*acZ,* white circle); right, input-output curve of AVPV-AAV-*Esr1* knockdown (black circle) vs KERKO (yellow circle) cells. **e,f,** percent of cells exhibiting DIB (**e**) or rebound bursts (**f)**. Cells per group is shown within or on top of the bar. g, representative action potentials at the rheobase from *lacZ* vs *Esr1* infected cells. **h-j**, individual values and mean±SEM rate of rise (**h**), full width at half maximum (FWHM, **i**) and afterhyperpolarization potential amplitude (AHP, **j**). * $p<0.05$ vs all other groups; # $p<-.05$ vs uninfected.

Figure 5 Deletion of ER in arcuate kisspeptin neurons **a**, Arc-AAV-*lacZ* and Arc-AAV-*Esr1* (g1 or g2) were bilaterally delivered to arcuate region (see Figure 5-figure supplement 1). Brain sections were processed to detect GFP (green), mCherry (red) and ERα (black). Arc-AAV-*Esr1* infected arcuate kisspeptin neurons exhibit decreased ERα expression compared to Arc-AAV-*lacZ* infected cells (right panel of each pair, white arrows indicate ERα-negative, magenta arrows indicate ERα-positive infected cells). **b**, representative reproductive cycles of mice that received Arc-AAV-*lacZ*, -*Esr1* g1 or g2; E, estrus, D, diestrus, P proestrus. Day 0 indicates the day of stereotaxic surgery. **c**, pulsatile LH release in Arc-AAV-*lacZ*, -*Esr1* g1 or g2 mice, # indicate pulse detected by Cluster analysis(Veldhuis and Johnson, 1986). **d**, mean±SEM days/week in proestrus before (from day -12 to day 14) and after infection (day 29 to day 56) in mice receiving Arc-AAV-*lacZ, -Esr1* g1 or g2. **e**, individual values and mean±SEM LH pulses/h. **f**, individual means and mean±SEM mean LH over the entire pretreatment sampling period. **g**, mean±SEM LH before (con) and 15 min after kisspeptin (kiss) injection (left) and before (con) and 15 min after GnRH injection (right). * $p<0.05$

Figure 6. *Esr1* knockdown in arcuate kisspeptin neurons alters cellular physiology. **a**, representative extracellular recordings of firing rate. **b**, **c**, individual values and mean±SEM firing rate (**b**) and percent of cells with firing rate >1 Hz (**c**); cells per group shown in bars. **d**, representative whole-cell recordings of EPSCs. **e, f,** individual values and mean±SEM of EPSC frequency (**e**) and amplitude (**f**). * $p<0.05$.

Figure 7. Schematic diagram of estradiol feedback regulation on ERα in AVPV and arcuate kisspeptin neurons in adulthood. Knockdown of ERα in AVPV kisspeptin neurons blunted LH surge but did not alter reproductive cyclicity whereas knockdown of ERα in arcuate kisspeptin neurons disrupted the cyclicity.

Figure 1-figure supplement 1 a, individual values and mean±SEM input resistance (R_{input}, **a**) and cell capacitance (Cm, **b**) for AVPV kisspeptin neurons in control and KERKO mice (left), in mice with AAV vector delivered to AVPV region (middle with *Esr1* status confirmed by either immunofluorescence (IF) single-cell qPCR (PCR) *post hoc)*, and in AVPV-AAV-*Esr1* infected mice (combined detection methods) vs KERKO mice (right). **c** individual values and mean±SEM normalized uterine mass (uterine mass/body mass, mg/g) of control and KERKO mice (left), of mice with AAV delivered to AVPV region, OVX+E (middle), and of mice with AAV delivered to arcuate region, intact (right). * $p<0.05$. The lack of a significant drop in the ratio is likely attributable to the short duration post OVX (2 days).

Figure 3-figure supplement 1. Bilateral delivery of AAV-*lacZ*, and AAV-*Esr1* (g1 and g2) to AVPV of adult female mice. Immunofluorescence was used to detect GFP (green), mCherry (red) and immunohistochemistry to detect ERα (black).

Figure 4-figure supplement 1. Single-cell qPCR for mRNA from AVPV kisspeptin neurons in mice with AAV vector delivered to AVPV region. Bar graphs show percentage of cell positive for each gene. * $p<0.05$, Fisher's exact test.

Figure 5-figure supplement 1. Bilateral delivery of AAV-*lacZ*, and AAV-*Esr1* (g1 and g2) to arcuate of adult female mice. Immunofluorescence was used to detect GFP (green), mCherry (red) and immunohistochemistry to detect ERα (black).

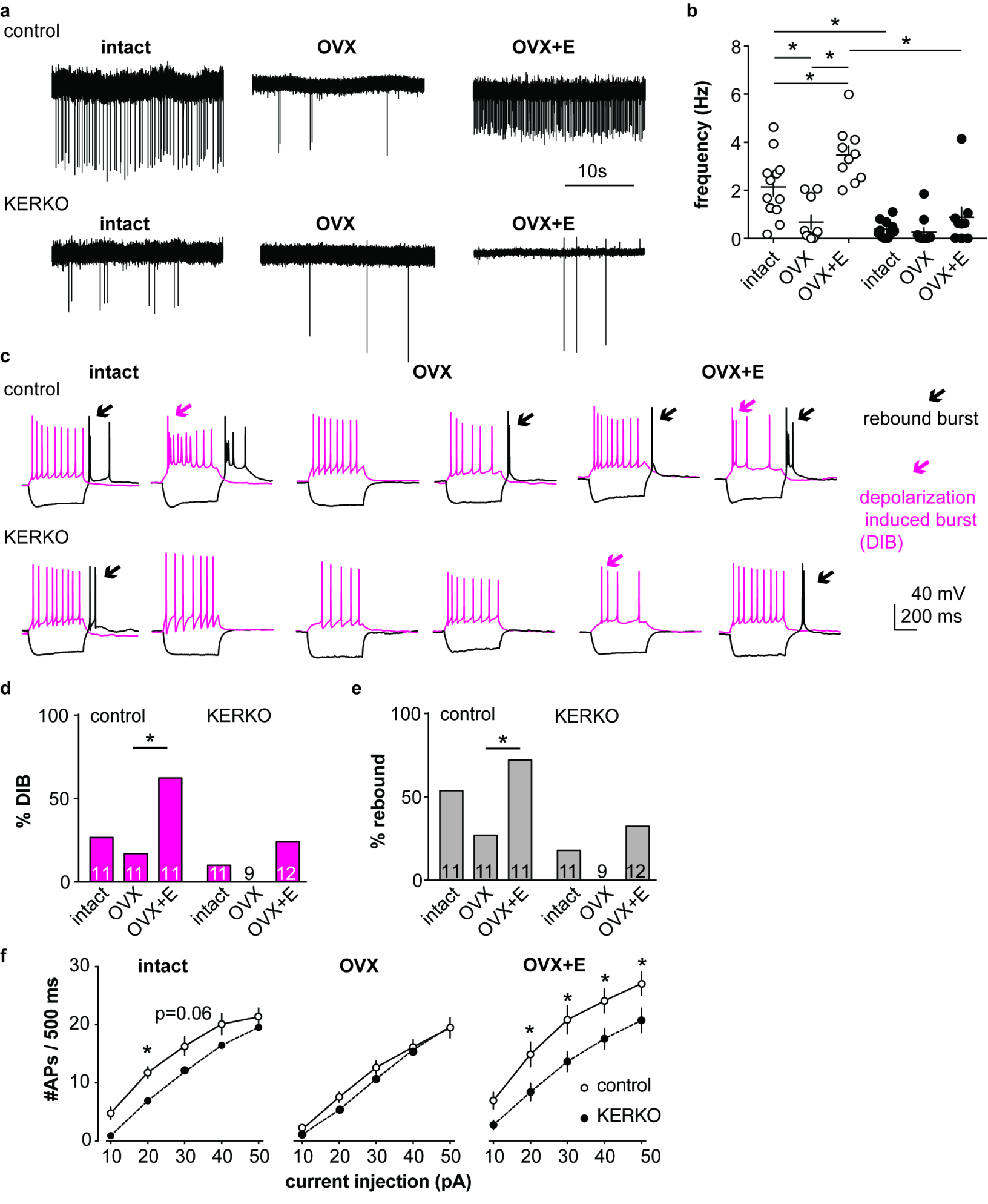
a
control
intact
OVX
OVX+E
10s
KERKO
intact
OVX
OVX+E
b
frequency (Hz)
intact
OVX
OVX+E
intact
OVX
OVX+E
c
intact
OVX
OVX+E
control
rebound burst
depolarization induced burst (DIB)
KERKO
40 mV
200 ms
d
% DIB
control
KERKO
intact
OVX
OVX+E
e
% rebound
control
KERKO
f
intact
OVX
OVX+E
p=0.06
#APs / 500 ms
control
KERKO
current injection (pA)

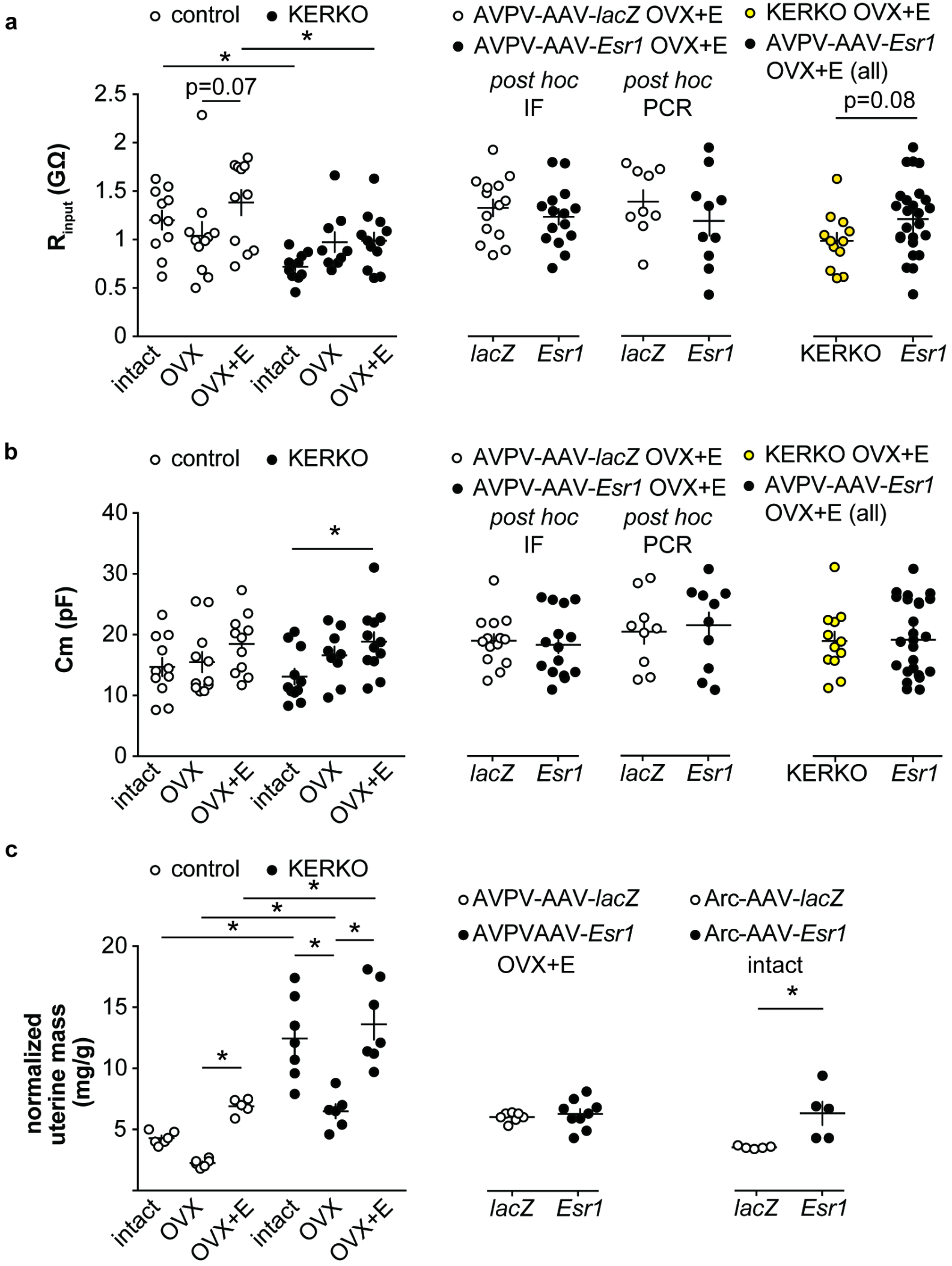
a
control
KERKO
*
*
p=0.07
2.5
2
1.5
1
0.5
0
R_{input} (GΩ)
intact
OVX
OVX+E
intact
OVX
OVX+E
AVPV-AAV-lacZ OVX+E
AVPV-AAV-Esr1 OVX+E
post hoc IF
post hoc PCR
lacZ
Esr1
lacZ
Esr1
KERKO OVX+E
AVPV-AAV-Esr1 OVX+E (all)
p=0.08
KERKO
Esr1
b
control
KERKO
*
40
30
20
10
0
Cm (pF)
intact
OVX
OVX+E
intact
OVX
OVX+E
AVPV-AAV-lacZ OVX+E
AVPV-AAV-Esr1 OVX+E
post hoc IF
post hoc PCR
lacZ
Esr1
lacZ
Esr1
KERKO OVX+E
AVPV-AAV-Esr1 OVX+E (all)
KERKO
Esr1
c
control
KERKO
*
*
*
*
*
20
15
10
5
normalized uterine mass (mg/g)
intact
OVX
OVX+E
intact
OVX
OVX+E
AVPV-AAV-lacZ
AVPVAAV-Esr1 OVX+E
lacZ
Esr1
Arc-AAV-lacZ
Arc-AAV-Esr1 intact
*
lacZ
Esr1

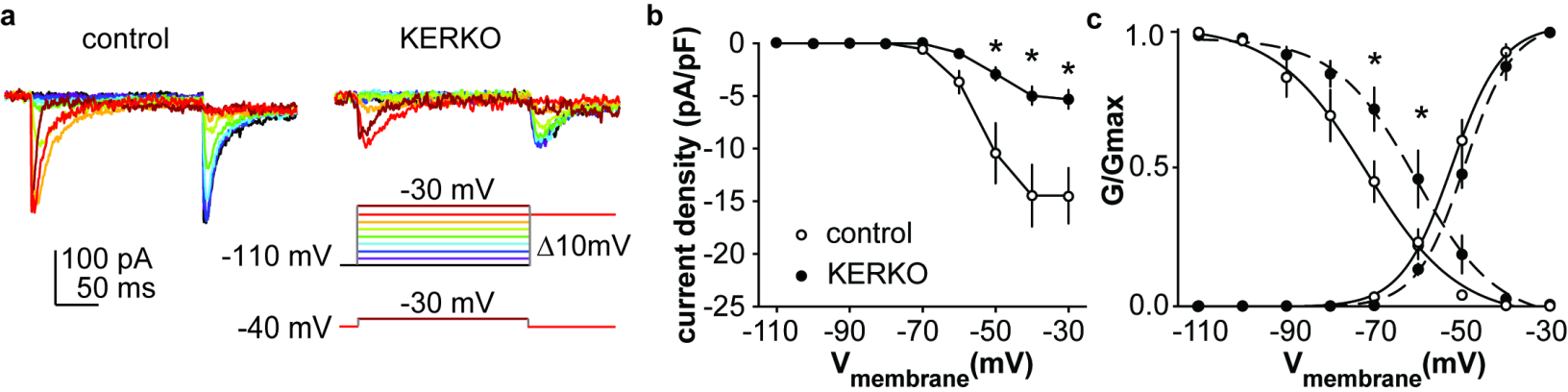
a
control
KERKO
100 pA
50 ms
-30 mV
-110 mV
Δ10mV
-30 mV
-40 mV
b
current density (pA/pF)
0
-5
-10
-15
-20
-25
control
KERKO
-110
-90
-70
-50
-30
V membrane (mV)
c
G/Gmax
1.0
0.5
0.0
-110
-90
-70
-50
-30
V membrane (mV)

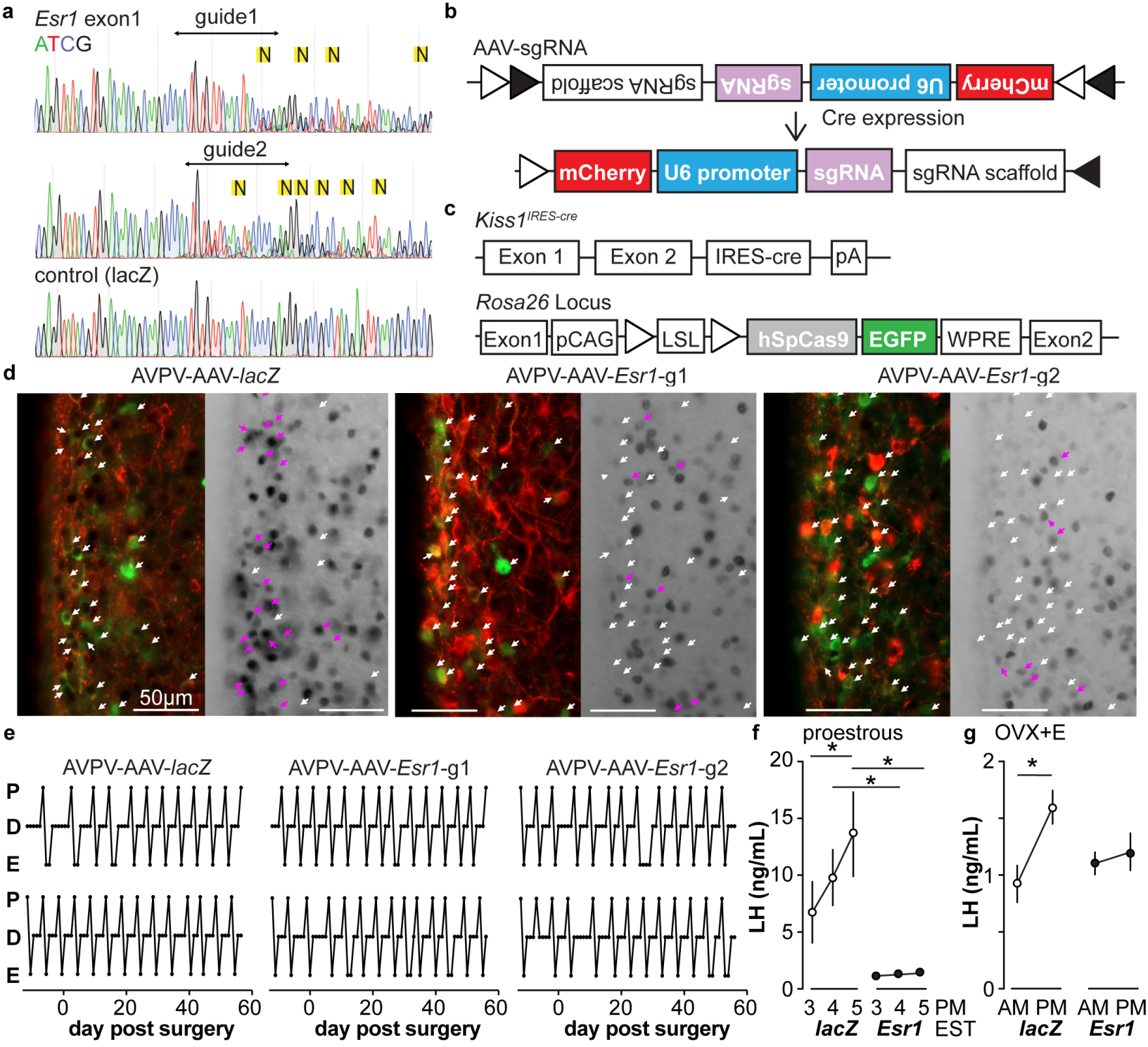
a
Esr1 exon1
ATCG
guide1
N N N N
guide2
N NN N N N
control (lacZ)
b
AAV-sgRNA
sgRNA scaffold
sgRNA
U6 promoter
mCherry
Cre expression
mCherry
U6 promoter
sgRNA
sgRNA scaffold
c
Kiss1IRES-cre
Exon 1
Exon 2
IRES-cre
pA
Rosa26 Locus
Exon1
pCAG
LSL
hSpCas9
EGFP
WPRE
Exon2
d
AVPV-AAV-lacZ
AVPV-AAV-Esr1-g1
AVPV-AAV-Esr1-g2
50μm
e
AVPV-AAV-lacZ
AVPV-AAV-Esr1-g1
AVPV-AAV-Esr1-g2
P
D
E
P
D
E
0 20 40 60
day post surgery
0 20 40 60
day post surgery
0 20 40 60
day post surgery
f
proestrous
LH (ng/mL)
20
15
10
5
0
3 4 5 3 4 5 PM
lacZ Esr1 EST
g
OVX+E
LH (ng/mL)
2
1
0
AM PM AM PM
lacZ Esr1

AVPV-AAV-*lacZ*

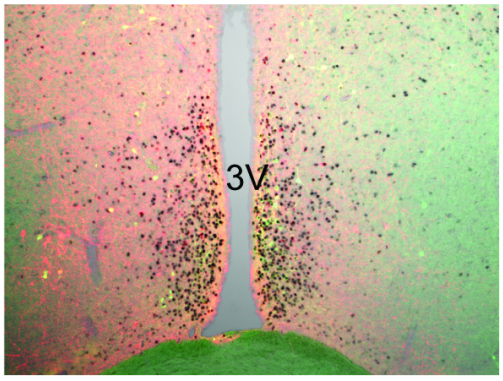

AVPV-AAV-*Esr1*-g1

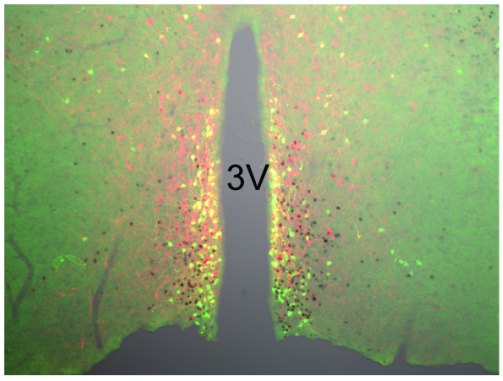

AVPV-AAV-*Esr1*-g2

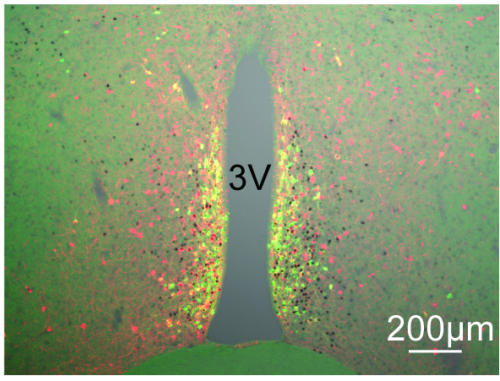

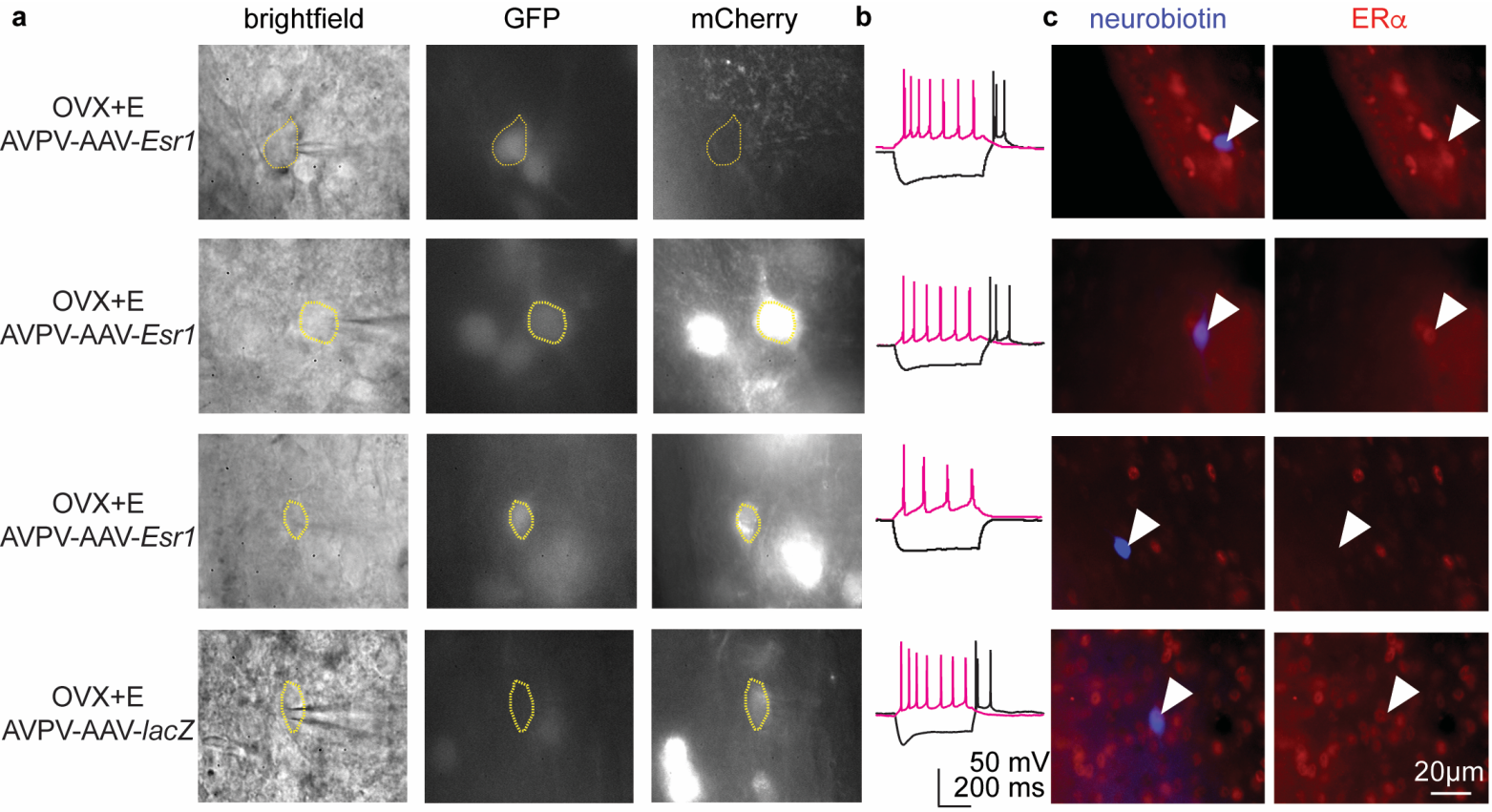
a
brightfield
GFP
mCherry
b
c
neurobiotin
ERα
OVX+E
AVPV-AAV-Esr1
OVX+E
AVPV-AAV-Esr1
OVX+E
AVPV-AAV-Esr1
OVX+E
AVPV-AAV-lacZ
50 mV
200 ms
20μm

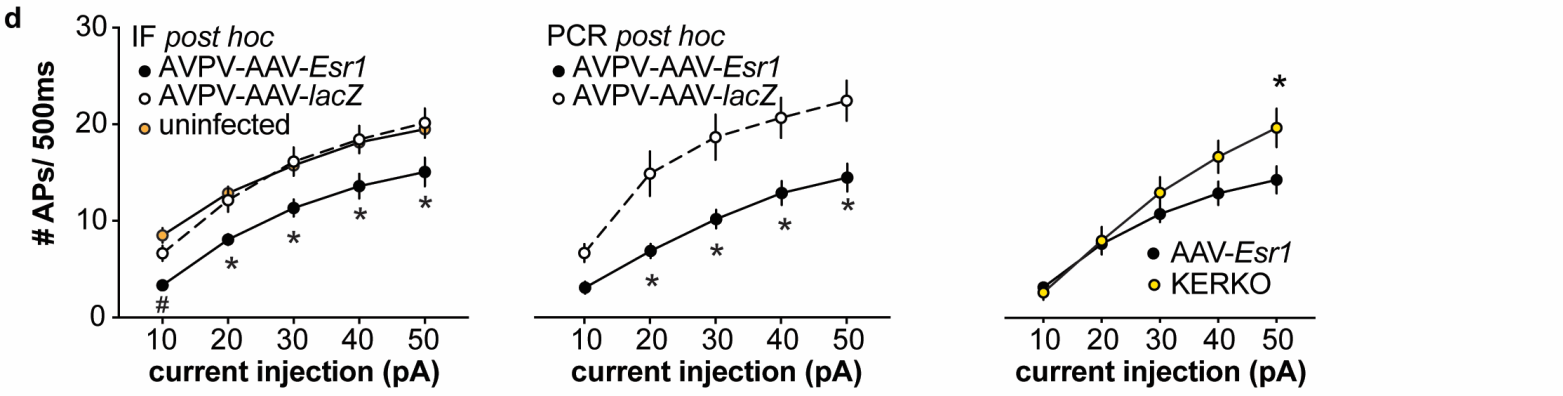
d
IF post hoc
AVPV-AAV-Esr1
AVPV-AAV-lacZ
uninfected
APs/ 500ms
current injection (pA)
PCR post hoc
AVPV-AAV-Esr1
AVPV-AAV-lacZ
current injection (pA)
AAV-Esr1
KERKO
current injection (pA)

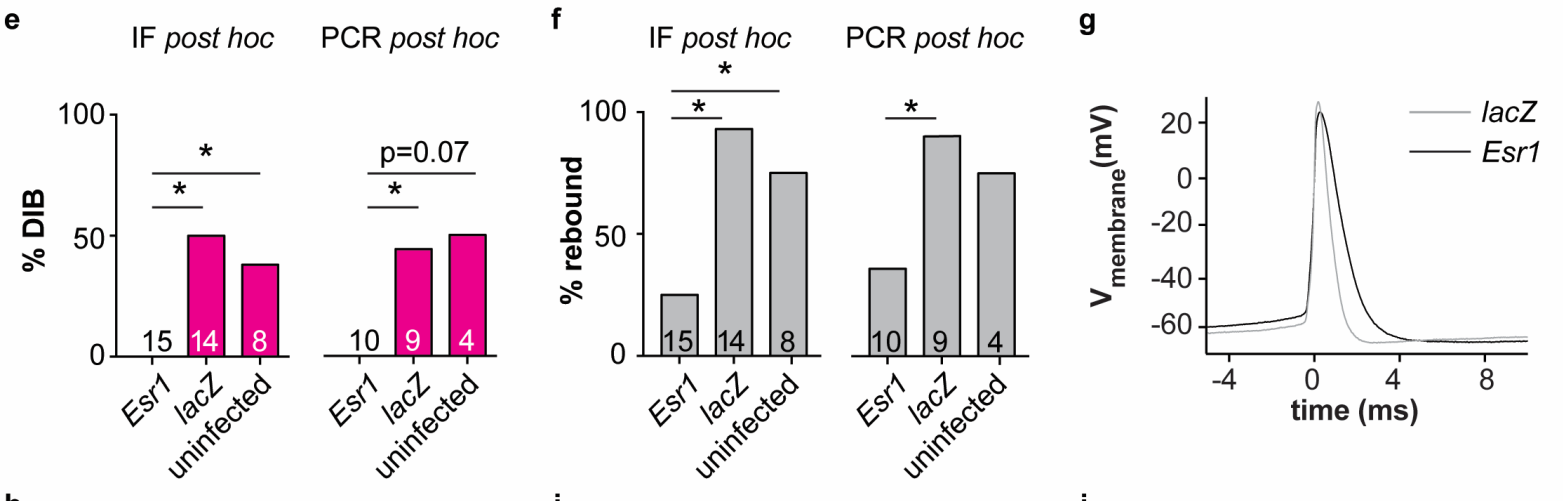
e
IF post hoc
PCR post hoc
% DIB
p=0.07
15
14
8
10
9
4
Esr1
lacZ
uninfected
f
IF post hoc
PCR post hoc
% rebound
g
lacZ
Esr1
V membrane (mV)
time (ms)

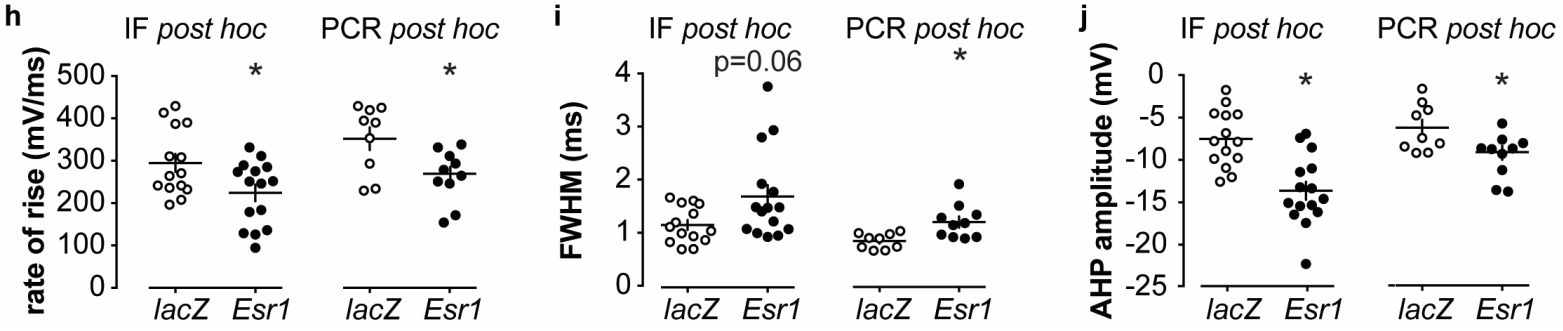
h
IF post hoc
PCR post hoc
rate of rise (mV/ms)
lacZ
Esr1
i
IF post hoc
PCR post hoc
p=0.06
FWHM (ms)
j
IF post hoc
PCR post hoc
AHP amplitude (mV)

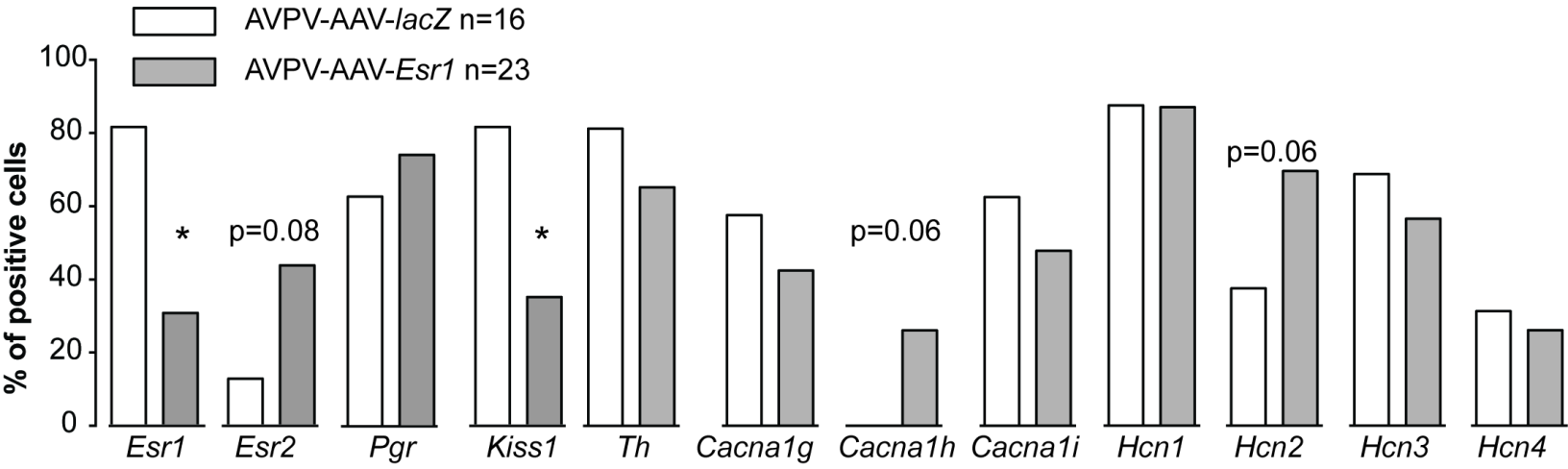
AVPV-AAV-lacZ n=16
AVPV-AAV-Esr1 n=23
% of positive cells
100
80
60
40
20
0
*
p=0.08
*
p=0.06
p=0.06
Esr1
Esr2
Pgr
Kiss1
Th
Cacna1g
Cacna1h
Cacna1i
Hcn1
Hcn2
Hcn3
Hcn4

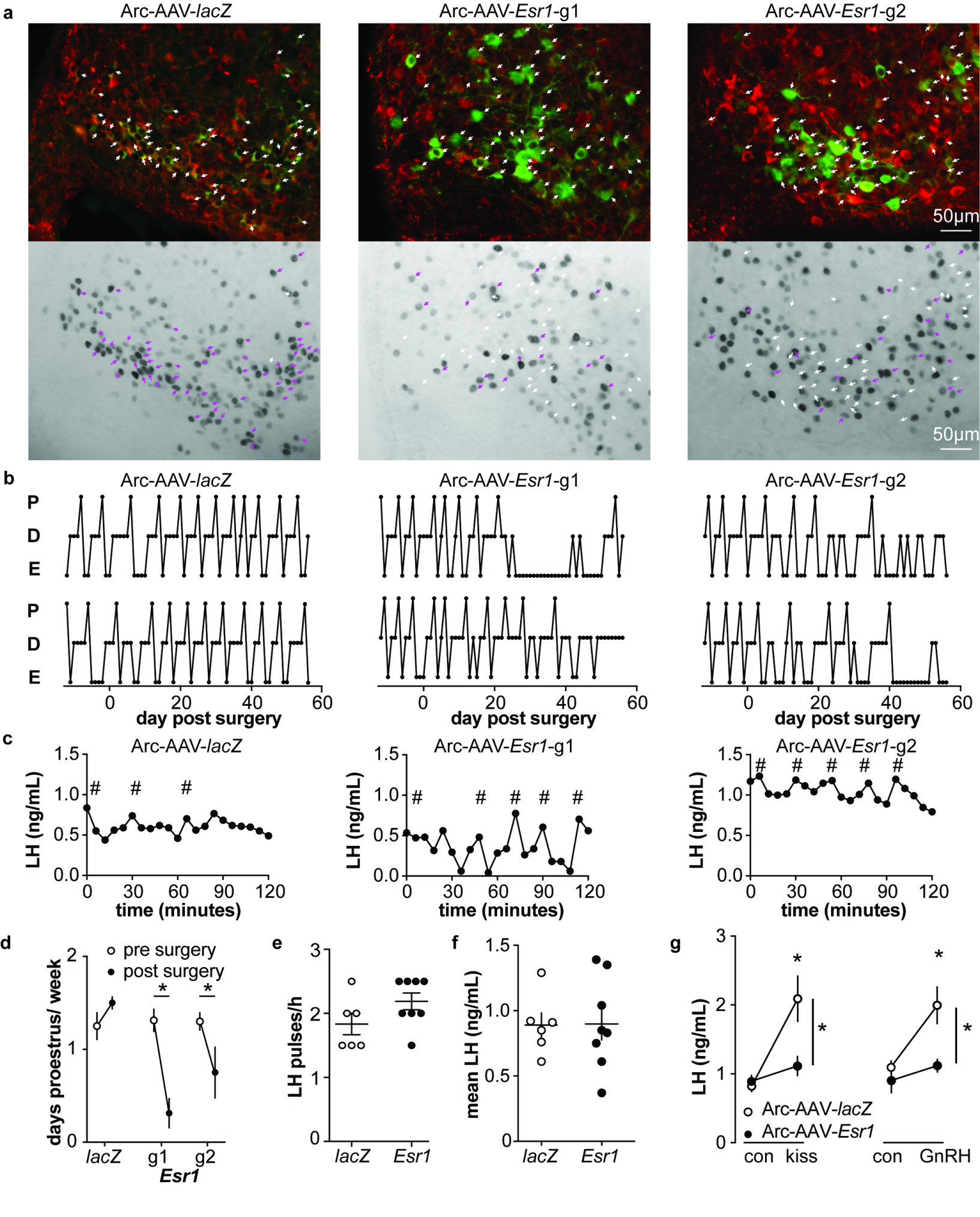
a
Arc-AAV-lacZ
Arc-AAV-Esr1-g1
Arc-AAV-Esr1-g2
50μm
50μm
b
Arc-AAV-lacZ
Arc-AAV-Esr1-g1
Arc-AAV-Esr1-g2
P
D
E
day post surgery
c
Arc-AAV-lacZ
Arc-AAV-Esr1-g1
Arc-AAV-Esr1-g2
LH (ng/mL)
time (minutes)
d
pre surgery
post surgery
days proestrus/ week
lacZ
g1
g2
Esr1
e
LH pulses/h
lacZ
Esr1
f
mean LH (ng/mL)
lacZ
Esr1
g
LH (ng/mL)
Arc-AAV-lacZ
Arc-AAV-Esr1
con
kiss
con
GnRH

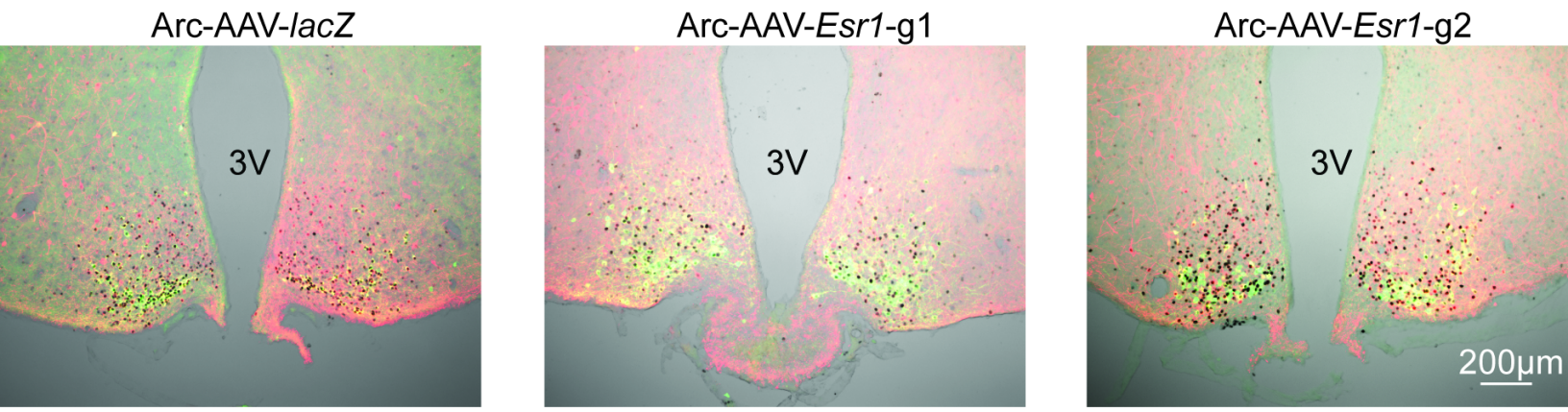
Arc-AAV-*lacZ*
3V
Arc-AAV-*Esr1*-g1
3V
Arc-AAV-*Esr1*-g2
3V
200μm

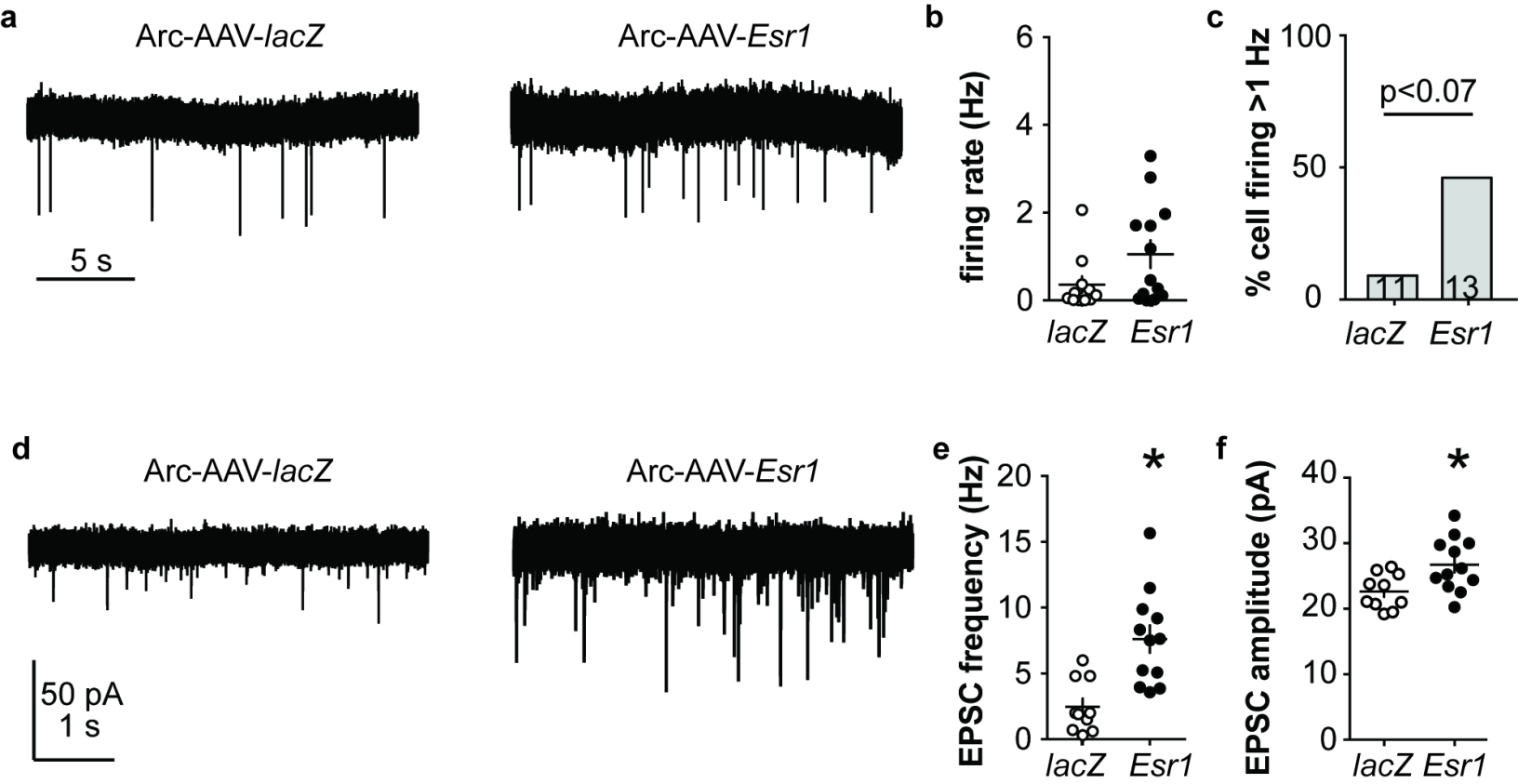
a
Arc-AAV-lacZ
Arc-AAV-Esr1
5 s
b
firing rate (Hz)
6
4
2
0
lacZ
Esr1
c
% cell firing >1 Hz
100
50
0
p<0.07
11
13
lacZ
Esr1
d
Arc-AAV-lacZ
Arc-AAV-Esr1
50 pA
1 s
e
EPSC frequency (Hz)
20
15
10
5
0
*
lacZ
Esr1
f
EPSC amplitude (pA)
40
30
20
10
0
*
lacZ
Esr1

in control adult female mice

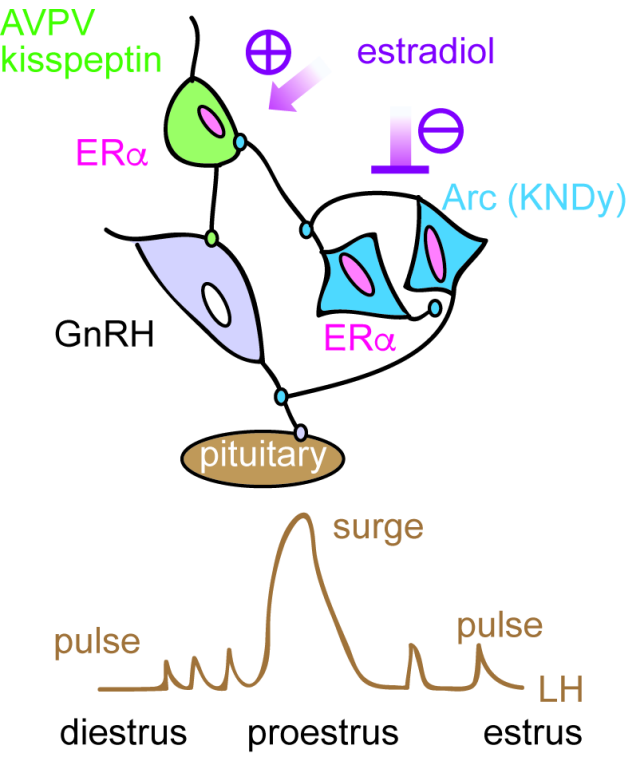

after CRISPR-Cas9 mediated ERα knockdown

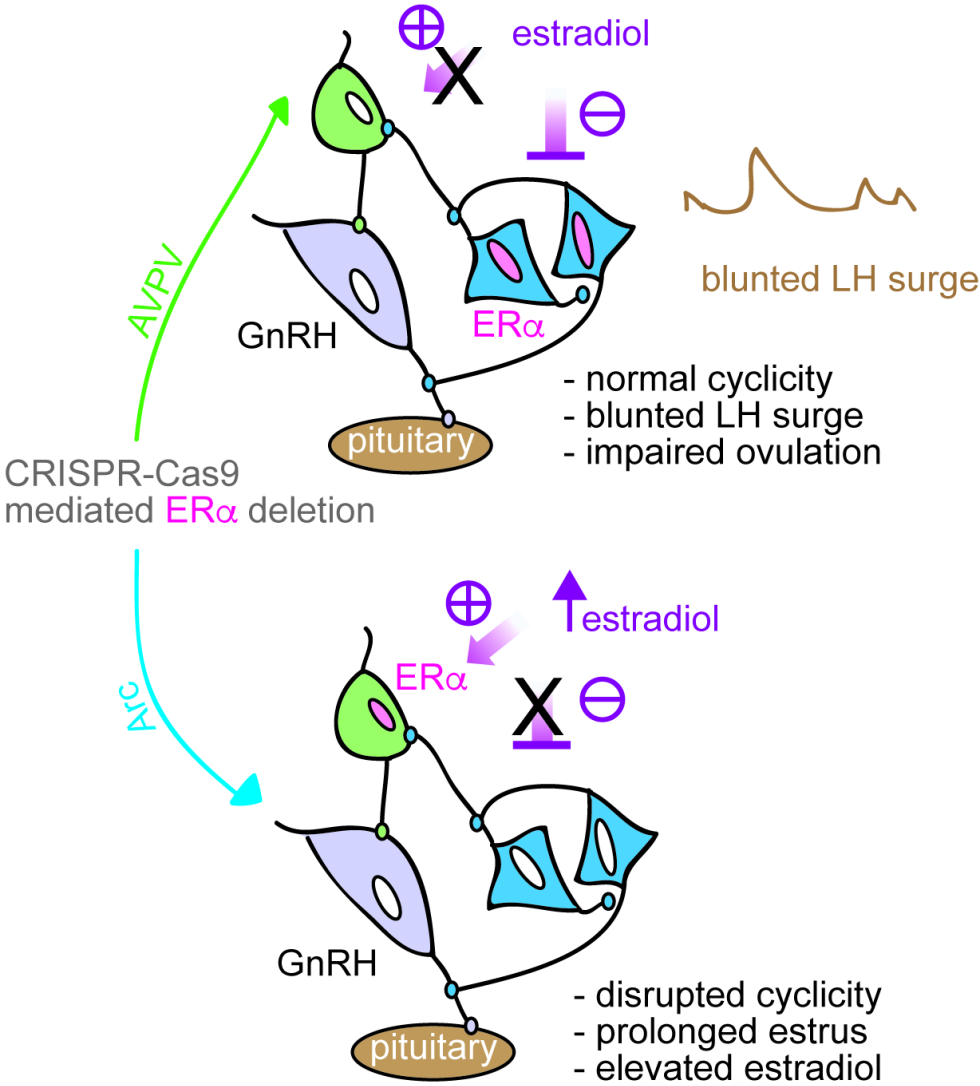

estradiol positive feedback

estradiol negative feedback

ERα